Journal of Molecular Structure 1248 (2022) 131418

Contents lists available at ScienceDirect

Journal of Molecular Structure

journal homepage: www.elsevier.com/locate/molstr

Novel quinoxaline derivatives of 2, 3-diphenylquinoxaline-6-carbaldehyde and 4, 4′-(6-methylquinoxaline-2,3-diyl)bis (N,N-diphenylaniline): Synthesis, structural, DFT-computational, molecular docking, antibacterial, antioxidant, and anticancer studies

J Irshad Ahamed [h,*], G.R. Ramkumaar [a], P. Kamalarajan [b], K. Narendran [c], M.F. Valan [d], T. Sundareswaran [e], T.A. Sundaravadivel [f], B. Venkatadri [g], S. Bharathi [h]

[a] Department of Physics, C. Kandaswami Naidu College for Men, Anna Nagar East, Tamil Nadu, India
[b] Department of Chemistry, R.M.D Engineering College, Kavaraipettai, Tamil Nadu 601206, India
[c] Department of Chemistry, Saveetha Engineering College, Thandalam, Chennai 602105, India
[d] Department of Chemistry, IFE (Loyola Institute of Frontier Energy), Loyola College, University of Madras, Nungambakkam, Chennai, Tamil Nadu, 600034, India
[e] Department of Physics, RMK College of Engineering and Technology, RSM Nagar, Puduvoyal, Tamil Nadu 601206, India
[f] Department of Mechanical, R.M.D Engineering College, Kavaraipettai, Tamil Nadu 601206, India
[g] Department of Plant Biology & Biotechnology, Loyola College (Autonomous), Chennai - 600 034, Tamil Nadu, India. (University of Madras)
[h] Department of chemistry. (SHIFT – II), C. Kandaswami Naidu College for Men, Anna Nagar East, Chennai, Tamil Nadu 600102, India

ARTICLE INFO

Article history:
Received 29 June 2021
Revised 30 August 2021
Accepted 31 August 2021
Available online 3 September 2021

Keywords:
New quinoxaline derivatives DPQC and MDBD
Spectral characterisation
DFT computational
In vitro Anticancer
Molecular docking

ABSTRACT

The quinoxaline derivatives of 2, 3-diphenylquinoxaline-6-carbaldehyde **(DPQC)** and 4, 4′-(6-methylquinoxaline-2,3-diyl)bis(N,N-diphenylaniline) **(MDBD)** were synthesized using direct condensation methods, and various spectral analysis were characterized by experimental and *ab initio* Density functional theory (DFT) theoretical methods at the B3LYP level with 6–311++G(d,p) basis sets were used for the different spectrum analysis, which included UV-Visible, Fourier-transform infrared spectroscopy (FTIR), and ^{1}H and ^{13}C nuclear magnetic resonance (NMR) chemical shifts. Furthermore, for these title molecules, Nonlinear Optical (NLO) was utilized to compute first-order hyperpolarizability (β) and Mulligan population analysis was performed. The ESI-Mass spectrum analysis was performed for these quinoxaline derivatives. In this study, title molecules of DPQC and MDBD were tested for *in vitro* antibacterial, antioxidant, and anticancer properties which exhibited enhanced biological activities. In particular, the title molecule MDBD gave enhanced anticancer activity at the lowest concentration of 125 µg/mL against human liver cancer (HepG2) cell lines, as well as potent bactericidal activity with a maximum of (19.5 ± 1.0 mm) at 2.5 µg/mL against *Yersinia enterocolitica* (MTCC 840). In an (H_2O_2) scavenging study, MDBD revealed potent antioxidant activity (64.21%). The DPPH radical scavenging antioxidant activity of MDBD was discovered at (67.48 %) concentration at 500 µg/mL. The best binding energy between anticancer target protein, specifically c-Met-kinase (hepatocyte growth factor; PDB ID: 3F66) and DPQC and MDBD compounds, were determined using in silico molecular docking. The auto dock software provided superior results for the title compound MDBD, which exhibited a higher ligand-receptor interaction energy value of -10.8 (kcal/mol) against 3F66 protein and a 0.01187 µM inhibition constant (ki) with (active site A) presented amino acids such as A: ARG1086, A: MET1211, A: VAL1092, A: ALA1226, A: ALA1108, A: MET1211. Further, studies are warranted to explore their promising anticancer and other pharmacological and biochemical properties.

1. Introduction

Cancer is the main cause of morbidity and mortality worldwide, which developed because of the unregulated increase in malignant cells which can spread to different organ systems. Liver cancer is one of the main predominant diseases important

* Corresponding author.
E-mail address: irshad@loyolacollege.edu (J.I. Ahamed).

https://doi.org/10.1016/j.molstruc.2021.131418
0022-2860/

for mortality in humans [1]. Quinoxaline is an essential heterocyclic nucleus created via the combination of two types of aromatic rings, which include benzene plus pyrazine (additionally known as benzopyrazine) [2,3]. The broad range of biological activities, including the antitumor activity of quinoxaline derivatives, is known and well documented in the literature [4,5]. The activity of quinoxalines as antitumor agents also showed potent and selective inhibition of human tyrosine kinase (TRK) in the liver cancer HepG2 [6]. N-(4-methyl-2-nitrophenyl)-2-(3-methyl-2-oxoquinoxalin-1(2H)-yl) acetamide has been reported as a potential antioxidant activity [7]. Antioxidant studies are important owing to their capability to stop disease development by reducing the damage caused by free radical oxidative stress in a patient [8]. Even if they started enhanced anticancer agents in the last thirty years, they have severe side effects from chemotherapy treatment and severe health problems, leading to death sometimes. Cancer remains a life-threatening sickness due to the shortage of valuable anticancer drugs and additionally creates effects of chemotherapy [9]. Therefore, efforts are still needed to increase great anticancer-causing agents to deal with most cancers successfully. The chemical compounds from the heterocyclic class play an essential role in modern drug discovery by structural modification to develop various compounds.

The search for a brand new quinoxaline agent for most cancer remedies is a crucial device within medicinal chemistry. In our current research work, the novel quinoxaline derivatives of 2,3-diphenylquinoxaline-6-carbaldehyde **(DPQC)** and 4, 4′-(6-methylquinoxaline-2,3-diyl)bis(N,N-diphenylaniline) **(MDBD)** have been recognized to behave as anticancer agents for human (HepG2) liver cancer cell lines and also completed the different spectroscopic evaluations by experimental and Density Function Theory (DFT) calculation with B3LYP/ 6–311++G (d,p) level. These quinoxaline derivatives are cost-effective and their initial materials are readily available. As quinoxaline moiety-containing molecules exhibit diverse organic significance, this study was interested in synthesizing the diverse quinoxaline derivatives and examining their anticancer effects utilizing *in vitro* and *in silico* approaches.

2. Materials and methods

2.1. Chemicals and reagents

In this study, the chemicals and reagents including benzil, 1,2-bis(4-(diphenylamino)phenyl)ethane-1,2-dione, 3,4-diaminobenzaldehyde, 4-methylbenzene-1,2-diamine, and MeOH (Sigma Aldrich, USA), Silica gel with a mesh of 60–120 (Merck, India), the pre-covered aluminium sheet of silica gel G/UV-254 of 0.2 mm thickness (Merck, Germany) were used for the synthesis of quinoxaline derivatives.

2.2. Spectral characterization

The synthesized compounds were recorded by the Fourier transform infrared (FT-IR) spectrum of the molecule was recorded employing a Perkin Elmer spectrometer fitted with a KBr beam splitter at around 4000–500 cm^{-1} with methanol solvent. The spectral measurements were completed by the Sophisticated Analytical Instrumentation Facility (SAIF), IIT, and Madras, India. The UV-Visible absorption spectra were taken on an Analytikjena specord 250 spectrophotometer. The NMR spectra (^1H and ^{13}C) were recorded on Bruker Avance (400 MHz and 100 MHz) in $CDCl_3$ solvent. The chemical shift value is confirmed in δ (ppm), and the coupling constant (J) is reported in Hz, and tetramethylsilane (Me4Si) is an internal standard. The mass spectrometry was done on a total ion chromatography (TIC) spectrometer. Elemental analysis was completed on the PerkinElmer CHNS/O 2400 series II elemental analyser (India). The Elemental (CHNS/O) analysis specified that the calculated and found values were within the acceptable limits (±0.4%). Reactions were observed using means of TLC utilizing precoated plates (Merck, India). Column chromatographic separation was done using silica gel with a mesh of 60–120.

2.3. Synthesis

2.3.1. General synthesis of novel quinoxaline derivatives are described in (Scheme 1) for ***dpqc*** and ***mdbd*** compounds

The different 1, 2- diamines such as 3,4-diaminobenzaldehyde and 4-methylbenzene-1,2-diamine 2 g, (18.49 mmol) in 20 mL of methanol, in addition to 3.8 g of different 1, 2-diketones such as benzil and 1,2-bis(4-(diphenylamino)phenyl)ethane-1,2-dione (18.49 mmol) were further added to the mixture. Then use a magnetic stirrer to stir the chemical mixture at room temperature vigorously. The progress of the reaction was monitored by thin-layer chromatography (TLC). The final product was quenched with water (10 mL) and ethyl acetate (EtOAc) (20 mL). The organic layer within the chemical mixture was isolated and dried out over anhydrous Na_2SO_4 to give a crude product. The product becomes isolated and purified using 60–120 mesh silica gel column chromatography using EtOAc 2:8 Hexane ratios.

2.4. Experimental data

2.4.1. 2, 3-diphenylquinoxaline-6-carbaldehyde ***dpqc***

Yield: 70 %; Light yellow; mp: 131- 132°C; IR (KBr, ν, cm^{-1}): 3437 cm^{-1} (OH stretching vibration), 3053, 3028, 2854 cm^{-1} (C-H stretching vibrations), 1618, 1483, 1444, 1344 cm^{-1} (Aromatic (C=C) stretching vibrations), 1201, 1138, 1058 (H-C-C bending vibrations), 1022, 979, 833, 773, 700, 545 cm^{-1} (H-C-C-C torsion vibrations), and 592 cm^{-1} (H-C-C bending vibrations); UV(λ_{max}, nm): 251 nm ($\pi \rightarrow \pi^*$) and 360 nm (n→ π^*); ^1H NMR (400 MHz, $CDCl_3$): δ 7.26–7.33(m, 6H) 7.46–7.49 (m, 4H), 8.18- 8.19 (d, J=2 Hz, 2H), 8.57 (s, 1H), 10.19 (s, 1H); ^{13}C NMR (100 MHz, $CDCl_3$): 126.77, 128.40, 129.32, 129.47, 129.82, 129.91, 130.46, 134.76, 137.06, 138.46, 140.86, 144.22, 154.78, 155.66, 191.36; Elemental Analysis calcd % for $C_{21}H_{14}N_2O$: C, 81.27; H, 4.55; N, 9.03; O, 5.16; Found %: C, 81.19; H, 4.48; N, 9.01; O, 5.08; MS (ESI) for $C_{21}H_{14}N_2O$: m/z 311.40 $[M+H]^+$.

2.4.2. 4, 4′-(6-methylquinoxaline-2,3-diyl)bis(N,N-diphenylaniline) ***mdbd***

Yield: 73%; Dark yellow; mp: 222–224°C;IR (KBr, ν, cm^{-1}): 3243, 3129 cm^{-1}(C-H stretching vibrations), 3004 cm^{-1} (C-H asymmetric methyl stretching vibration), 1672, 1607, 1117, 1084cm^{-1} (C=C stretching vibrations), 1417cm^{-1} (C-N stretching vibration), 1368, 1228 cm^{-1} (H-C-C bending vibrations), 973, 902, 804, 703cm-1 (H-C-C-C torsion vibrations), 653cm^{-1} (C-C-C bending vibration); UV (λ_{max}, nm): 314nm($\pi \rightarrow \pi^*$), 371, 470nm(n→ π^*); ^1H NMR (400 MHz, $CDCl_3$): δ 2.50 (s, 3H), 6.93–6.96 (m, 4H), 7.09–7.10 (d, J = 1.2 Hz, 8H), 7.25–7.31 (m, 12H), 7.58–7.60 (dd, J = 1.2, 1.2 Hz, 1H), 7.90–7.91 (d, J = 1.6 Hz, 1H), 8.03–8.04 (d, J = 5.6 Hz, 4H), 8.28–8.30 (d, J = 6 Hz, 1H); ^{13}C NMR (100 MHz, $CDCl_3$): δ 21.68, 122.90, 124.87, 126.26, 126.36, 128.86, 129.79, 129.95, 131.62, 132.41, 140.11, 140.80, 141.24, 145.42, 147.06, 153.52, 154.22; Elemental Analysis calcd % for $C_{45}H_{34}N_4$: C, 85.68; H, 5.43; N, 8.88; Found %: C, 85.51; H, 5.34; N, 8.76; MS (ESI) for $C_{45}H_{34}N_4$: m/z 631.73 $[M+H]^+$.

2.5. Computational details

The density functional theory has achieved tremendous significance in quantum chemical computation. The present research

exploration was performed with the B3LYP (Beckee-3- Lee-Yang-Parr) method, (Gaussian 09 program) package [10] as well as included the 6–311++G (d,p) basis set. In the DFT study, the *ab*-initio method of molecular calculating properties has recently been enhanced [11]. Initially, the geometry was optimized, followed by the calculation of geometrical parameters and the vibrational assignments. To avoid the systematic errors caused by basis set incompleteness, negligence of electron correlation and vibrational anharmonicity, a general scaling factor of 0.961was used to scale the computed wavenumbers. Additionally, the computed vibrational frequencies were revealed through the potential energy distribution (PED) investigation of all the fundamental vibration modes reported by the Vibrational Energy Distribution Analysis (VEDA) [12,13] program. The isotropic shielding values were used to calculate the isotropic chemical shifts (δ) for tetramethylsilane (TMS). The UV–visible spectra and excited state dipole moment were calculated by the B3LYP method of the time-dependant DFT (TD-DFT) using a 6–311++G (d, p) basis set based on the optimized structure [14–16]. The Frontier molecular orbital energies (FMOs) [17], Mulliken's population analysis and molecular electrostatic potential calculations were carried out and the results are discussed. The molecular structures were visualized with the help of Gauss View [18]. The Gauss Sum 3.0 program has been used to obtain calculated FT-IR images [19]. The NLO properties of **DPQC** and **MDBD** like dipole moment (μ), polarizability ($\Delta\alpha$) and first-order hyperpolarizability (β) were carried out by the Gaussian 09 modelling package [20]. The ^{1}H and ^{13}C NMR isotropic shielding was computed using the GIAO method [21,22] and standardized parameters attained using the B3LYP/6–31G++ (d,p) technique. $\delta_{iso}(X) = \sigma_{TMS}(X)$- $\sigma_{iso}(X)$, where δ_{iso}isotropic chemical shift plus σ_{iso} isotropic shielding.

2.6. In vitro *antibacterial activity*

The gram-positive microbes *Staphylococcus aureus* (MTTC 3615), *Enterococcus faecalis* (MTCC 439), and the gram-negative bacteria *Yersinia enterocolitica* (MTCC 840) and *Proteus mirabilis* (MTCC 1771) from the American type cell culture reference bacterial strain (ATCC) were exploited for biological analysis with antibacterial test assays. The Gram-positive bacteria cultures were grown selectively on Nutrient broth (pH 7.0), whereas Mueller–Hinton broth (pH 7.0) was used for culturing Gram-negative bacteria. The cultures were incubated at 37 °C for 24 h in a rotator shaker. After a necessary period of incubation, the bacterial cultures (1.5 × 108 CFU/mL) were swabbed onto sterile Mueller Hinton agar plates. The synthesized quinoxaline derivatives of (25 mL) **(DPQC and MDBD)** were transferred to sterile discs (6 mm) and allowed to soak for 10–15 min. With the aid of tweezers dipped in ethanol, the disks were aseptically transferred to the plates seeded with the respective pathogens, flamed, and incubated at 37 °C for 24 hours. After 24 hours, the zone of inhibition (mm) formed by the combination of an organic compound was measured relative to the pathogenic bacteria index. Streptomycin and an appropriate disk immersion solvent were used as positive and negative controls, correspondingly. The experiments were completed in triplicate [23].

2.7. In vitro *antioxidant activity (H_2O_2 and dpph radical scavenging activity)*

The antioxidant property was evaluated using an H_2O_2 scavenging assay. The title molecules (DPQC) and (MDBD) at different concentrations from 100 to 1000 μg/mL prepared in ethanol were added to 0.6 mL of H_2O_2 solution. After 15 min of incubation, the absorbence of the reaction mixture was read at 230 nm. The blank solution includes H_2O_2 solution without any compound. The H_2O_2 scavenging activity of synthesized compounds was measured by hydrogen peroxide scavenging.

$$\text{Hydrogen peroxide scavenging}\,(\%) = (A_0 - A_1)/A_0 \times 100$$

Where, A_0 is the absorbence of the control, and A_1 is the absorbence of the sample.

The 1,1-diphenyl-2-picrylhydrazine (DPPH) method was utilized to analyse the antioxidant potential of synthetic compounds based on scavenging free radicals. In this process, 0.1 mM ethanol DPPH was prepared and added to the solution of quinoxaline derivatives. The different concentrations of (DPQC) and (MDBD) range from 100 to 500 μg/ml. It was then incubated for 30 minutes and the absorbence at 517 nm was assessed via a Beckman spectrophotometer. After incubation, the discolouration was calculated using an accurate blank of 517 nm. Protect from light for 30 minutes at 30 °C in the dark. Assessments were made in triplicate. D-ascorbic acid was employed as the standard. The DPPH was absorbed at 517 nm, and its reduced concentration used in antioxidant activity. The following formula measures the percentage of free radical scavenging activity of the quinoxaline derivatives.

$$\text{Scavenging}\,\% = \frac{1 - -A_{sample} - A_{blank}}{A_{control}} \times 100$$

Here, ethanol (3 mL) with the solution sample (0.1 ml) has utilized as the blank, and 3 ml of DPPH solution with EtOH (0.1 ml) was utilized as the negative control.

2.8. In vitro *anticancer activity*

The liver cancer (HepG2) cell line was served to test the anticancer activity of the compounds (DPQC) and (MDBD). Cells were cultured and maintained in Minimal Essential Media (MEM) (Hi-Media, India) supplemented with 10% foetal bovine serum (FBS) (Cistron Labs), Trypsin, MTT (methyl thiazolyl diphenyl-tetrazolium bromide), and dimethylsulfoxide (DMSO) (Himedia, India). The (HepG2) cells were incubated at 37 °C in a 5% CO_2 atmosphere; they were regularly subcultured and maintained in 2% MEM. A confluent monolayer of HepG2 cells was trypsinized and suspended in 10% MEM. 100μL of cell suspension was transferred to 96 well plates followed by 10% MEM was added and the plate was incubated at 37 °C in a 5% CO_2 environment. Various concentrations of molecules were prepared as 100 μg/mL, 50 μg/mL, 25 μg/mL, 12.5 μg/mL, 6.25 μg/mL, 3.125 μg/mL, 1.56 μg/mL and 0.78 μg/mL and transferred to the 96 well plates. Finally, 100 μL of 2% MEM was added. The morphological changes of (HepG2) cells were monitored every 24 h for three days and finally, the changes were noted after 72 h of the period. The highest concentration that did not show cellular toxicity was measured as the maximum non-toxic concentration of the compound. The cytotoxicity concentration was approved using the MTT (3-(4, 5-dimethylthiazol-2-YL)-2, 5-diphenyltetrazolium bromide) assay. In this assay, after 72 h of incubation of 96 well plates, 20 μL of MTT solution (5 mg/mL) was further added to all the wells and the plate was inculpated at 37 °C with 5% CO_2 for 4 hrs. After 4 hours of incubation, the medium presented in the plate was carefully removed without disturbing the cell monolayer. Finally, a volume of 120 μL of DMSO was added to the wells to dissolve the formazan crystals and read at 510 nm and 650 nm. The formula used to calculate the percentage of cell viability was the percentage of cell viability = treated x 100 %/untreated.

2.9. Molecular docking

Human c-Met-Kinase **(PDB code: 3F66)** complex with quinoxaline inhibitor was chosen as a protein target for docking investigations. The X-ray diffraction resolution of 3F66 was 1.4 Å. [24], and all molecular docking calculations were performed on Auto

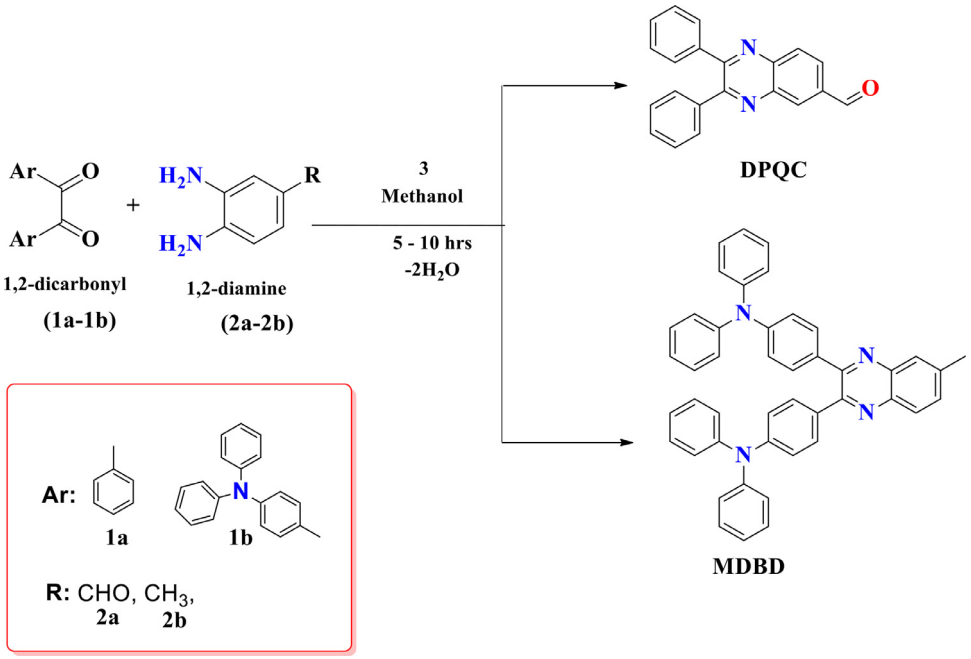

Scheme 1. A synthetic method for quinoxaline derivatives **DPQC** and **MDBD.**

Dock-Vina software. Co-crystallized ligands, water, and co-factors were removed before preparing the protein for docking. The Auto Dock Tools (ADT) graphical user interface is used to calculate Kollman's charge and polar hydrogen. The Lamarck Genetic Algorithm (LGA) function of Auto Dock software is used in the docking process [25]. *In Silico*, molecular docking investigations were finished by Autodock4.2. Docking analysis was accomplished with the flexible ligand and the rigid receptors. The x, y, z size grid box size values are 126 × 90 × 126, and the grid box centre x, y, z values are -12.08 x -22.198 × 28.788 with 0.542 Å grid spacing at the location of binding for the 3F66- Protein. The newly synthesized organic molecules (DPQC) and (MDBD) ligand structures were drawn by ChemDraw 12.0 software. The synthesized structure of the 2D compound is converted to mol format and then converted to 3D. Auto Dock uses the framework for the docking process [25]; all these ligands are purified and obtained through the selected twist tree using the Auto Dock ligand tool, selecting the torsion tree-choose root, and torsion tree-detect root. The final purified ligand is stored through the opening in pdbqt format for further use in molecular docking studies. Use Discovery Studio software [26] to perform visualization results.

3. Result and discussion

3.1. Chemistry

The novel derivatives of quinoxaline such as from **DPQC** and **MDBD** were achieved using direct condensation reaction between 1, 2-dicarbonyl **(1a-1b)** and 1,2-diamine **(2a-2b)** with the solvent MeOH **3** in the condition of mild acidity without using any catalyst [27,28]. The complete reaction was given in Scheme 1, which obtained final products with a significant yield percentage of 70%-73%. We explored the influence of electronic components of 1,2-diamine on the reaction results. It has been observed that 1,2-diamine bearing an electron-donating group (-Me) on the benzene ring, ***e.g.*** 4-methylbenzene-1,2-diamine **(2b)** with 1,2-dicarbonyl and the related product **MDBD**, was synthesized in excellent yields. However, the occurrence of an electron-withdrawing group in the benzene ring decreased the reactivity of the substrate. Some biologically essential compounds are shown in Fig. 1.

3.2. Molecular geometry

Figs. 2 and 3 shows the optimized structure of the title compounds **DPQC** and **MDBD**. Table S1-S4 (Supporting information) presents their bond lengths and bond angles computed using an optimized structure basis set of 6–311G++ (d, p) by the DFT method. The minimum energies optimized for the structure of title molecule **DPQC** is calculated by the HF/6–311G++ (d, p) and B3LYP/6–311G++ (d, p), with their values of -986.778 *a.u.* and - 993.424 *a.u.* The energy difference value is -6.65*a.u.*, whereas the title compound **MDBD** HF/6–311G++(d,p) and B3LYP/6–311G++(d,p) minimum energy values are -1940.973 *a.u.* and -1953.819*a.u.* with their energy difference value of -12.85 *a.u.* The novel compound MDBD has shown more energy difference than DPQC.

3.3. Atomic charges

The charge distribution mainly influences the vibration spectrum of the molecule. The total atomic charges of the title compounds **DPQC and MDBD** were obtained by the methods of Mulliken [29] and NBO using HF/6–311G++(d,p) and B3LYP/6–311G++(d,p). The theoretical level is shown in Figs. S1 and S2 (Supporting information). Total atomic charge values were achieved by Mulliken population investigation and natural charges were discovered by natural bond orbital analysis. The charge distribution is according to the linear combination of atomic orbitals and thus the wave function of the molecule. All hydrogen atoms have positive Mulliken charge values.

The molecule of the **DPQC** has atomic charges for the hydrogen atom that range from HF/6–311G++ (d, p) of 0.228 to 0.205, whereas B3LYP/6–311G++(d,p) ranges from 0.150 to 0.131. Because of polarization, the charges change with the basis set. For example, the charge of N14 atom values is -0.437 for B3LYP/6–311G++ (d,p) and -0.568 for HF/6–311G++ (d, p). The charge of N15 atom values is -0.439 for B3LYP/6–311G++(d,p) and -0.576 for HF/6–311G++ (d, p). Finally, the O38 atom values are -0.393 for B3LYP/6–311G++(d,p) and -0.522 for HF/6–311G++(d,p), as given in Table S5 (Supporting information). Table S5 concluded that the **DPQC** molecule presented nitrogen and oxygen atoms are exhib-

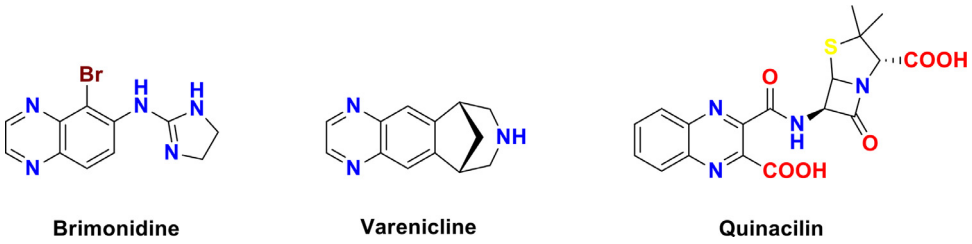

Fig. 1. Biologically important compounds of Quinoxaline.

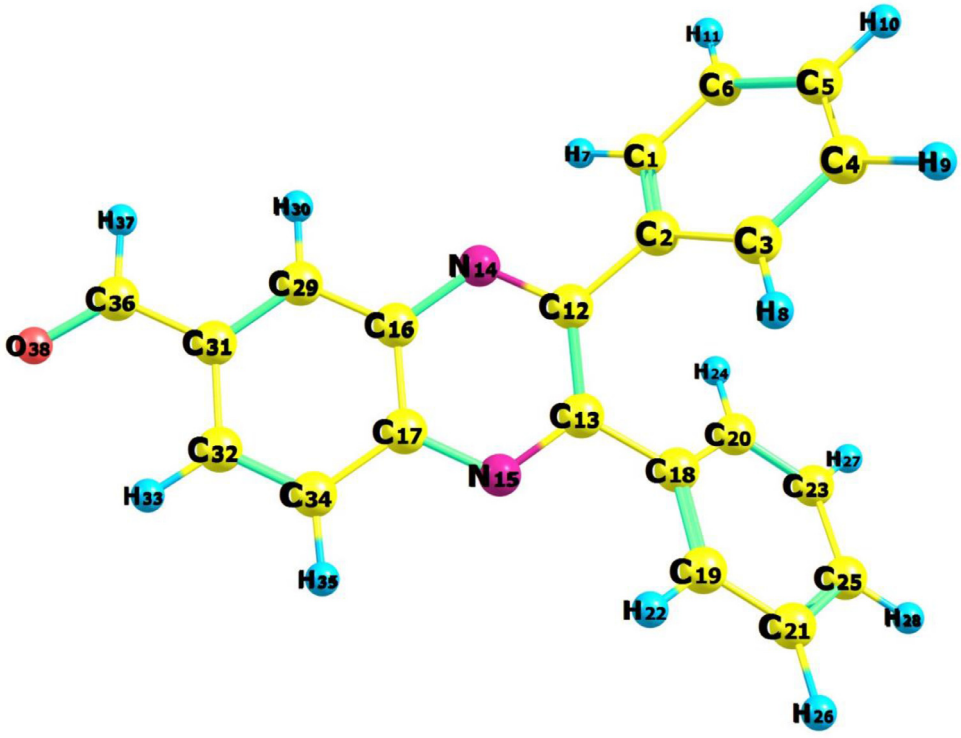

Fig. 2. Optimized structure of the title compound **DPQC.**

ited as a substantial negative charge, which is a donor atom. The C12, C13, C16, C17, and C36 hydrogen atoms were exhibited positive charges, which is an acceptor atom.

The molecule of the MDBD and its atomic charges for hydrogen atom HF/6–311G++ (d,p) is 0.241 to 0.229, wherein B3LYP/6–311G++ (d, p) ranges from 0.144 to 0.094. Because of polarization, the charges of N13 atom values is -0.430 for B3LYP/6–311G++ (d, p) and -0.604 for HF/6–311G++ (d, p), N14 atom values is -0.431 for B3LYP/6–311G++(d,p) and -0.591 for HF/6–311G++ (d, p), N38 atom values is -0.722 for B3LYP/6–311G++ (d, p) and -1.103 for HF/6–311G++ (d, p). Finally, the N39 atom values are -0.713 for B3LYP/6–311G++ (d, p) and -1.103 for HF/6–311G++ (d, p), as given in Table S6 (Supporting information). Table S6 concluded that the **MDBD** molecule contained nitrogen atoms with a significant negative charge, indicating that they were donor atoms. The C5, C11, C12, C15, C16, and C40 hydrogen atoms were exhibited as a positive charge, an acceptor atom.

3.4. Vibrational analysis

The vibration level of the identified compounds, especially **DPQC** and **MDBD**, is achieved by the DFT level (B3LYP), which is a way to approach the compound vibration level [30]. These molecules have been given 108 for **DPQC** and 243 for **MDBD** by positive value modes of vibrations for the confirmation of current synthesized compounds, with their geometry positioned at accurate local minima of the potential energy surface. The calculated wavenumbers are normally superior to the corresponding experimental ones because of electron correlation consequences and inadequate basis set deficiencies. Therefore, to enhance the calculated values, the discrepancy between experimental and theory is eliminated by computing a harmonic correction explicitly, through initiating a scalar field, using scaling of the computed wavenumbers with the right scaling factor [31–33].

The calculated wavenumbers (scaled), observed and assignments of FT-IR bands for these two synthesized title molecules are given in Table S7 and S8 (Supporting information), and comparison between calculated and observed wavenumbers FT-IR are shown in Fig. 4 for **DPQC** and Fig. 5 for **MDBD**. The calculated FT-IR images have been demonstrated by the Gauss Sum 3.0 program [19]. As detected from the correlation graphs, the FT-IR correlation coefficient of **DPQC** and **MDBD** (CC) R^2 values are 0.99494 and 0.99947 at the B3LYP/6–311G++(d,p) level. The computed and experimental FT-IR correlation coefficient spectrum images were revealed in Fig. S3 for **DPQC** and Fig. S4 for **MDBD**. The computed frequencies match the experimental FT-IR values well. The following vibration modes of these two new title molecules were discussed.

In our current research work, the title molecule **DPQC** experimental FT-IR (O-H) stretching vibration assigned at 3437cm^{-1} **(mode number 108)** with a PED contribution value of 96%,

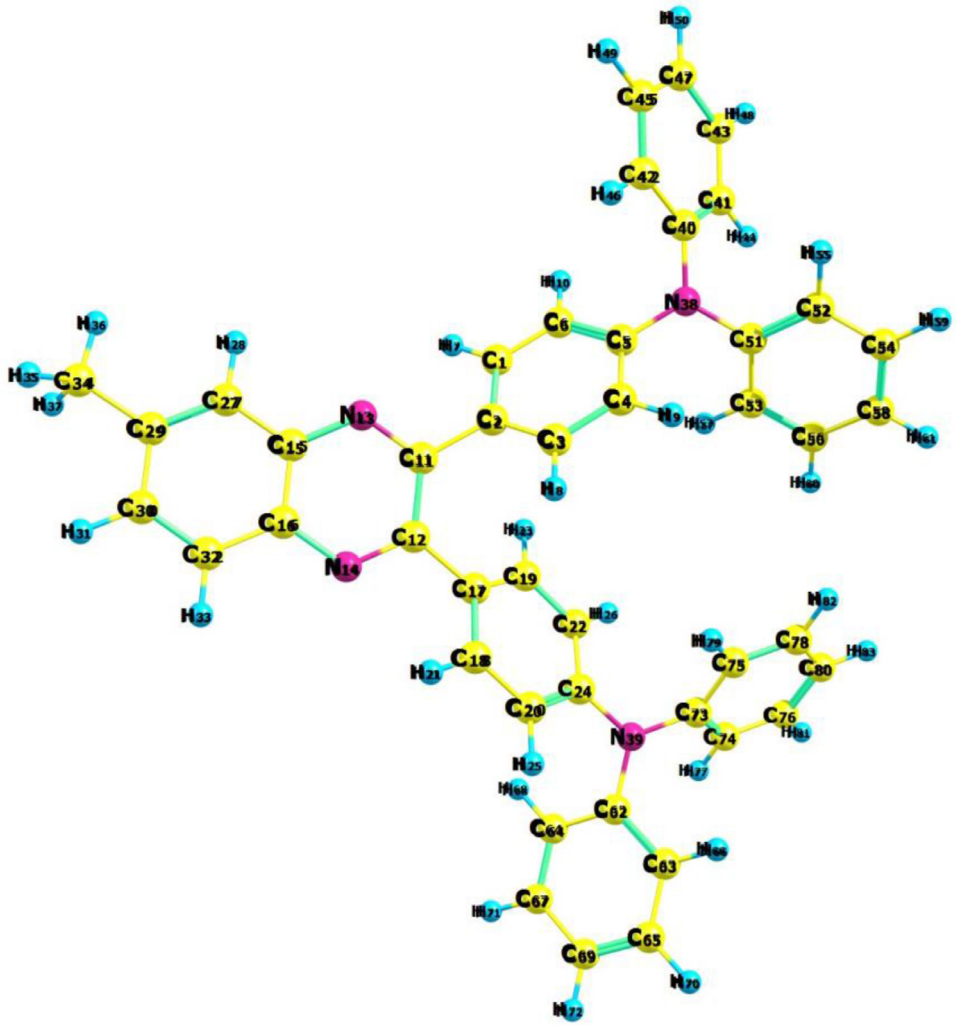

Fig. 3. Optimized structure of the title compound **MDBD.**

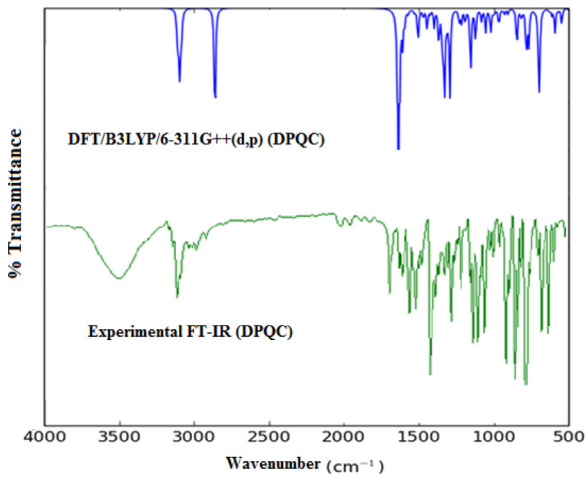

Fig. 4. Experimental and Theoretical vibrational spectra of **(DPQC).**

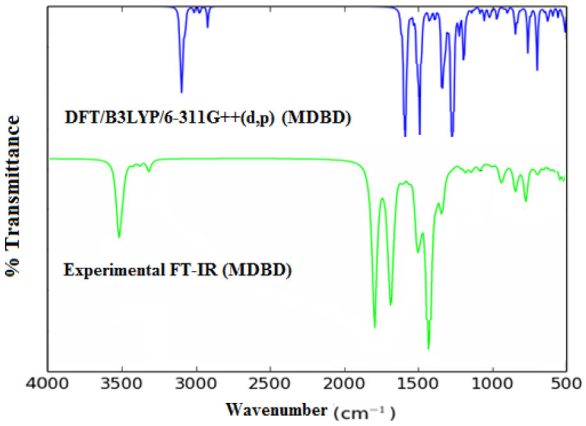

Fig. 5. Experimental and Theoretical vibrational spectra of (**MDBD**).

which is perfectly matched with the computed vibrational band at 3241cm^{-1}, respectively. According to the literature [34,35]. The aromatic C-H stretching vibrations occur. The substituent's nature never affects the bands in this region [36]. The compound **DPQC** experimental C-H stretching vibrations obtained in the range of 3053, 3028, and 2854cm^{-1} with **(mode numbers of 98, 97, and 115)** are also related to C-H stretching and coincide well with the calculated frequency values of 3205, 3095, and 2976cm^{-1} with a 79%, 87%, and 99% PED contribution. The title molecule **MDBD** experimental C-H stretching vibration detected in the range of 3243 and 3129cm^{-1} with **(mode numbers of 242 and 213)** are also related to C-H stretching and coincides a good deal with the calculated frequency values of 3239 and 3193cm^{-1} with a 16%, and

13% PED contribution, respectively, as per the literature [37]. Several bending vibrations, including β HCC, were observed in the 1563 to 125cm^{-1} range [38]. In our current analysis, the compound **DPQC** experimental FT-IR bending β HCC vibrations were discovered at 1201, 1138, 1058, and 592cm^{-1} with a PED contribution value of 15, 13, 15, and 47%. The compound **MDBD** experimental FT-IR bending β HCC vibrations are revealed at 1368 and 1228cm^{-1} with a PED contribution value of 49 and 16%. Furthermore, various β CCC bending and τ HCCC torsion vibrations were achieved in **DPQC** and **MDBD** compounds, which have been extensively studied [39–41]. The compound **MDBD** C-H stretching in pure (CH_3) methyl stretching vibration was obtained experimentally at 3004cm^{-1} with a **mode number of 210**. This is also reasoned to methyl stretching and coincides well with the calculated frequency values of 3038cm^{-1} with an 89% PED contribution. These frequency values were intimately in concord with the same modes in literature [42–44]. The compound **DPQC** experimental wavenumbers at 1618, 1483, and 1444cm^{-1} observed in the FT-IR spectrum were assigned to C=C stretching vibrations **(mode numbers of 89, 81, and 80)** PED contribution values of 17, 63, and 51% in the current work. The compound **MDBD** experimental FT-IR show C=C stretching vibrations at 1672, 1607, 1117, and 1084cm^{-1} with a PED contribution value of 28, 17, 25, and 14%, respectively **(mode numbers of 209, 199, 136, and 133)**. These frequency values were closely in agreement with the same modes in literature [45,46]. These two title molecules have achieved excellent concord with the calculated data given in Tables S7 and S8. The **MDBD** title compound experimental wavenumber was obtained at 1417 cm^{-1} for C-N stretching vibrations. The theoretical scaled wavenumber was found at 1485cm^{-1} with a **mode number of 181** for C-N stretching vibrations with a PED contribution value of 22%, respectively. The suitable vibration ranges were obtained in the literature [20]. This amine group raises the reactivity of the linked aromatic ring and acts as a wonderful neurotransmitter due to its electron-donating character.

3.5. Ultraviolet-Visible spectral analysis

The absorption spectroscopy of many organic molecules is based on transitions $\pi \rightarrow \pi^*$ and n$\rightarrow \pi^*$ in the UV-Visible region [47–49]. The UV-Visible spectral analysis was performed to understand the electronic transitions of the quinoxaline derivatives of 2, 3-diphenylquinoxaline-6-carbaldehyde **(DPQC)** and 4, 4′-(6-methylquinoxaline-2,3-diyl)bis (N,N-diphenylaniline) **(MDBD)** molecules. The UV-Visible spectrum was theoretically calculated by a 6–311++G(d,p) basis set for the gas phase. The experimental absorption spectra of the DPQC and MDBD molecules were recorded using methanol as a solvent. The overlap of experimental and theoretical calculated UV-Visible spectra was presented in Figs. S5 and S6 (Supporting information).

In the UV–Vis spectrum of compound **DPQC**, only two bands are shown at 251 nm and 360 nm. The experimental values of 251 nm and 360 nm correlate with DFT/B3LYP/6–311++G(d,p) calculated values of 230.31 nm and 354.74 nm, respectively, attributed to HOMO-2→LUMO+2 and HOMO-4→LUMO, which have electronic transition contribution values of 35% and 75%. The electronic transitions in DPQC are due to $\pi \rightarrow \pi^*$ and n$\rightarrow \pi^*$ transitions. In the compound **MDBD**, only three bands are shown at 314 nm, 371 nm, and 470 nm. The experimental values of 314 nm, 371 nm, and 470 nm correlate with DFT/B3LYP/6–311++G(d,p) calculated values at 308.53 nm, 352.10 nm, and 450.05 nm, respectively, attributed to HOMO→LUMO+3, HOMO-1→LUMO+1, and HOMO →LUMO, which have electronic transition contribution values of 52%, 36%, and 98%. The electronic transitions in MDBD are due to $\pi \rightarrow \pi^*$ and n$\rightarrow \pi^*$ transitions [50,51].

The DPQC and MDBD molecules experimental absorption wavelengths (energies) and computed electronic values, such as absorption wavelength (λ), energy gap (E), oscillator strength (f), and assignments of electronic transitions are mentioned in Table 1. The band gap energy was estimated by the $E = hc/\lambda$ formula. Here, h and c are constant; λ is the cut-off wavelength [52,53]. Table 1 shows the calculated and experimental wavelengths from absorption using methanol as a solvent, the % contribution from each transition, transition energies, and oscillator strength computed at the B3LYP/6–311G++ (d,p) level for DPQC and MDBD in the gas phase.

3.6. Frontier molecular orbitals (FMOs) analysis

The orbits (LUMO-Lowest Unoccupied Molecular Orbital) and (HOMO-Highest Occupied Molecular Orbital) are used for the calculation of band gap energy and structures stability. The compounds with a large HOMO and LUMO energy gap are often considered hard, whereas compounds with a small energy gap are soft and much more reactive [55]. The computational method results are shown in Table S9 (Supporting information), which was estimated by HOMO-LUMO energies, energy gap (ΔE), ionization potential (I), electron affinity (A), absolute electro-negative (χ), and softness (S) of the **DPQC and MDBD** molecules. $I = -E_{HOMO}$ and $A = -E_{LUMO}$, respectively, where I and A are the ionization potentials and electron affinities. In this inspection, the relations between the DPQC molecule of E_{HOMO} and E_{LUMO} are -6.2613 (eV) and -2.4165 (eV), as well as the relations between MDBD molecule of E_{HOMO} and $E_{LUMO,}$ are -4.8438 (eV) and -1, 7226 (eV) shown in Fig. 6a and Fig. 7a also show FMOs, where the positive phase is revealed in red and the negative phase is revealed in green, and these images showed the occurrence of intramolecular charge transfer between the **DPQC** molecule and the **MDBD** molecule. In this research, these compounds were shown to have a low band gap energy value of LUMO-HOMO **(Gap (eV) = 3.8448)** for the DPQC molecule and **(Gap (eV) = 3.1212)** for the MDBD molecule. This low energy gap indicates charge transfer inside the compound. The stable structure is identical to the band gap of bioactive molecules [56]. Fig. 6**a** and Fig. 7**a** suggest that the ionization potential value of I = 6.2613 (eV) for the DPQC molecule and I = 4.8438 (eV) for MDBD molecules are required to eliminate an electron from the HOMO.

The lower value of electron affinity A = 2.4165 (eV) for the DPQC molecule and A = 1.7226 (eV) for the MDBD molecule shows that these two compounds have accepted electrons for reaction. As a result of having LUMO and HOMO, molecular energy values, electronegativity, chemical hardness, and other values can be estimated by the following formula. $\chi = I+A/2$ (Electronegativity), $\mu = -(I+A)/2$ (Chemical potential), $\eta = I-A/2$ (Chemical hardness), $S=1/2\eta$ (chemical softness), and $\omega=\mu^2/2\eta$ (Electrophilicity index).

The Gauss-sum 3.0 program [19] was employed to simulate the density of states (DOS) spectrum, which provides a visual representation of captured orbitals, virtual orbitals, HOMO and LUMO energy levels, and band gap of the DPQC and MDBD molecules. The green and red lines in the DOS spectrum imply occupied and virtual orbitals, respectively. Fig. 6**b** and Fig. 7**b** show the DOS spectrum of the DPQC molecule and MDBD molecule, respectively.

3.7. Molecular electrostatic potentials (MEP)

The molecular electrostatic potential (MEP) uses colour grading to depict molecule shapes, size, and electrostatic potential. The MEPs map and contour plots are valuable tools for evaluating molecular structures and their physicochemical properties, as well as drugs [57]. It provides information on a molecule's chemical reactivity. The electrophilic or nucleophilic properties are explained

Table 1
Theoretical and experimental electronic transition parameters of **DPQC** and **MDBD** using a TD-DFT/6–311G++(d,p) method in gas phase and their assignments.

Molecules	Transition	Experimental λ_{max}(nm)	Band gap (eV)	Theoretical λ_{max}(nm)	Band gap (eV)	Oscillator strength (*f*)	Transitions with % of contributions Assignment [54]
DPQC	$\pi \rightarrow \pi^*$	251	4.941	230.31	5.3834	0.0213	HOMO-2 → LUMO+2 (35%)
	n→ π *	360	3.445	354.74	3.4951	0.001	HOMO - 4 → LUMO (75%)
MDBD	$\pi \rightarrow \pi^*$	314	3.940	308.53	4.0186	0.2586	HOMO → LUMO +3 (52%)
	n→ π *	371	3.3424	352.1	3.5213	0.1411	HOMO-1 → LUMO+1 (36%)
	n→ π *	470	2.6383	450.05	2.7549	0.2357	HOMO → LUMO (98%)

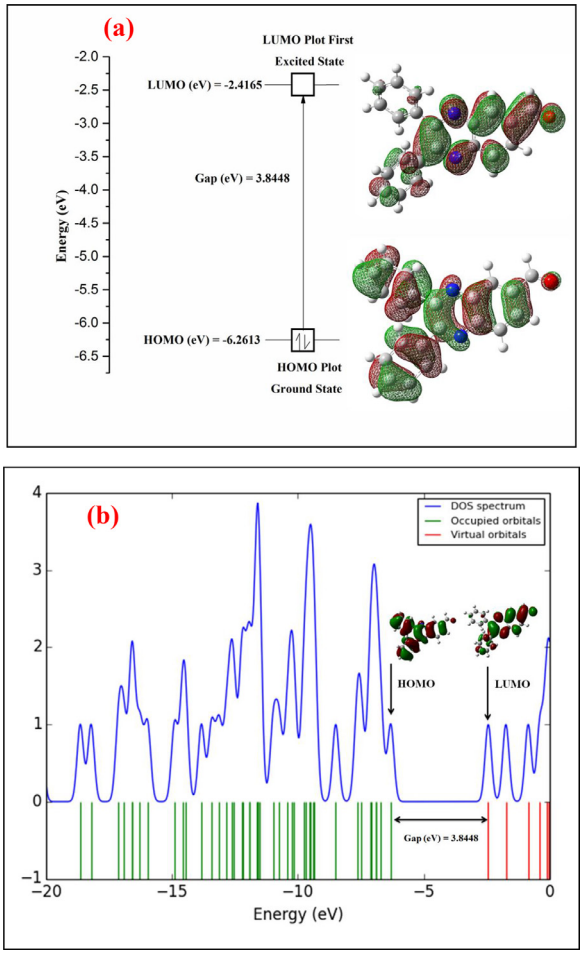

Fig. 6. **(a)** The frontier molecular orbitals of the **DPQC** molecule. **(b)** Density of States spectrum of the **DPQC** molecule.

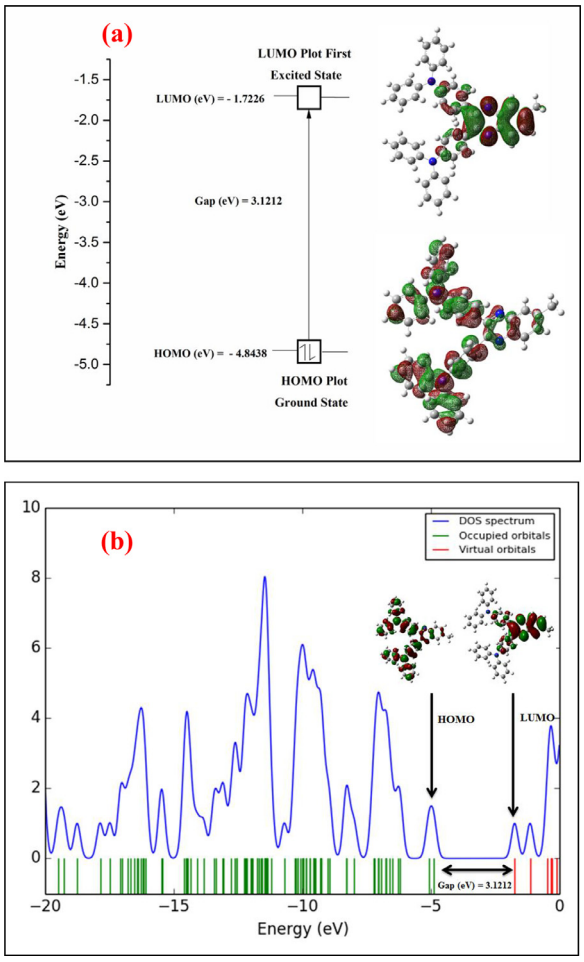

Fig. 7. **(a)** The frontier molecular orbitals of the **MDBD** molecule. **(b)** Density of States spectrum of the **MDBD** molecule.

using the electrostatic potential created surrounding a molecule via the distribution of charges [58].

Figs 8 and 9 show the **DPQC and MDBD** title compounds MEPs map generated by the optimized figure using the Gauss View 5.0 software. Different colours show the diverse values of the electrostatic potential: red denotes the highest negative electrostatic potential, blue denotes positive electrostatic potential, and green denotes the portion of zero potential. The bulk of the light green region of the MEP surface seems like a possibility between the two extremes of red and dark blue. The negative regions of molecular electrostatic potential indicate that the assessed electron density in the molecule attracts the proton (red shade). The repulsion of protons by atomic nuclei is represented by the positive electrostatic potential (shades of blue). The MEP map confirms that the negative potential areas are around oxygen and nitrogen, while the positive potential areas are around hydrogen atoms, as per these estimated outcomes. The compound **DPQC** with the carbonyl group (C=O) shows red colours in Fig. 8 and the **MDBD** compound with the nitrogen groups N13 and N14 shows red colours in Fig. 9, indicating that the compound negative regions (nucleophilic reactive sites) are areas that easily interact with proteins for biological activity. The hydrogen atoms in **DPQC and MDBD** compounds are coloured blue, indicating an electrophilic reactive site, and yellow, indicating a lower electrostatic potential. The diagram of the MEP illustrates the electrostatic potential for decreasing compound surfaces based on red > orange > yellow > blue [59,60], the following spectrum of colours.

3.8. Nonlinear optical properties

The polarizability values will determine the NLO properties [61] and the Nonlinear Optical properties (NLO) activity values of linear polarizability (α), total molecular dipole moment (μ), and first-order hyperpolarizability (β). The anisotropy of the polariz-

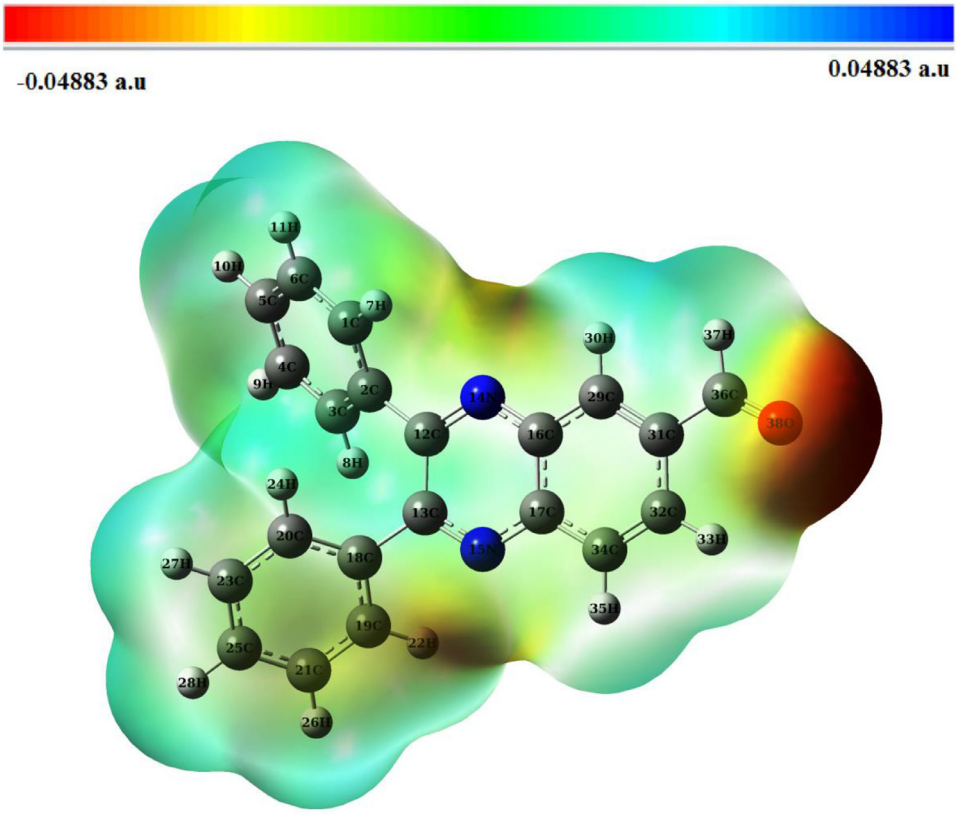

Fig. 8. Molecular Electrostatic Potential (MEP) of **DPQC**.

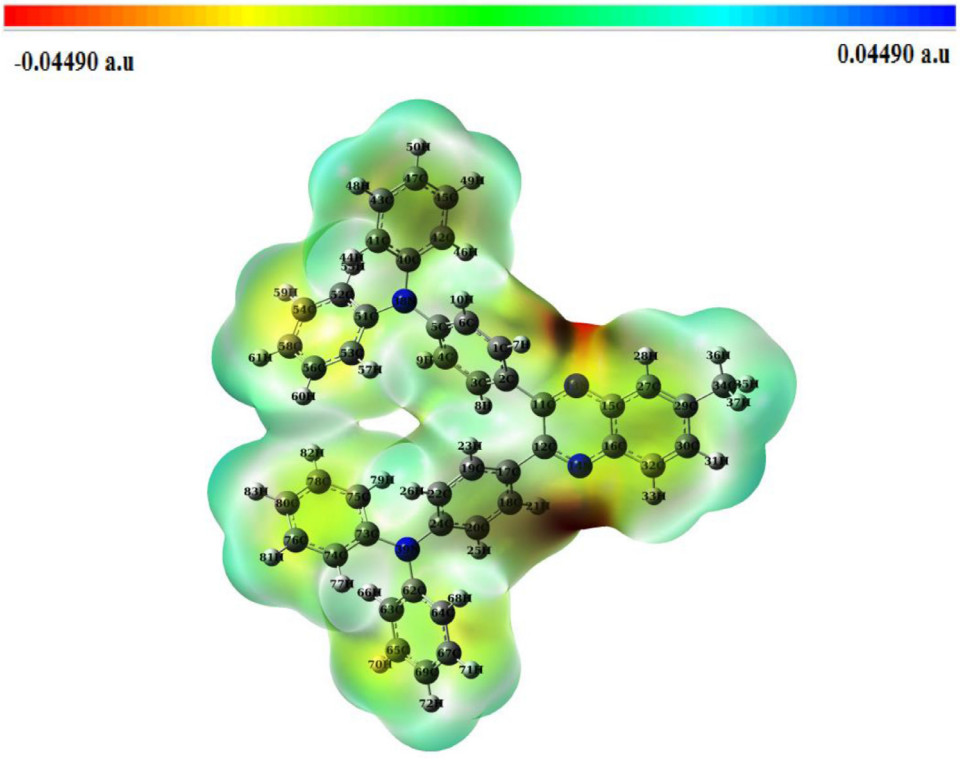

Fig. 9. Molecular Electrostatic Potential (MEP) of **MDBD**.

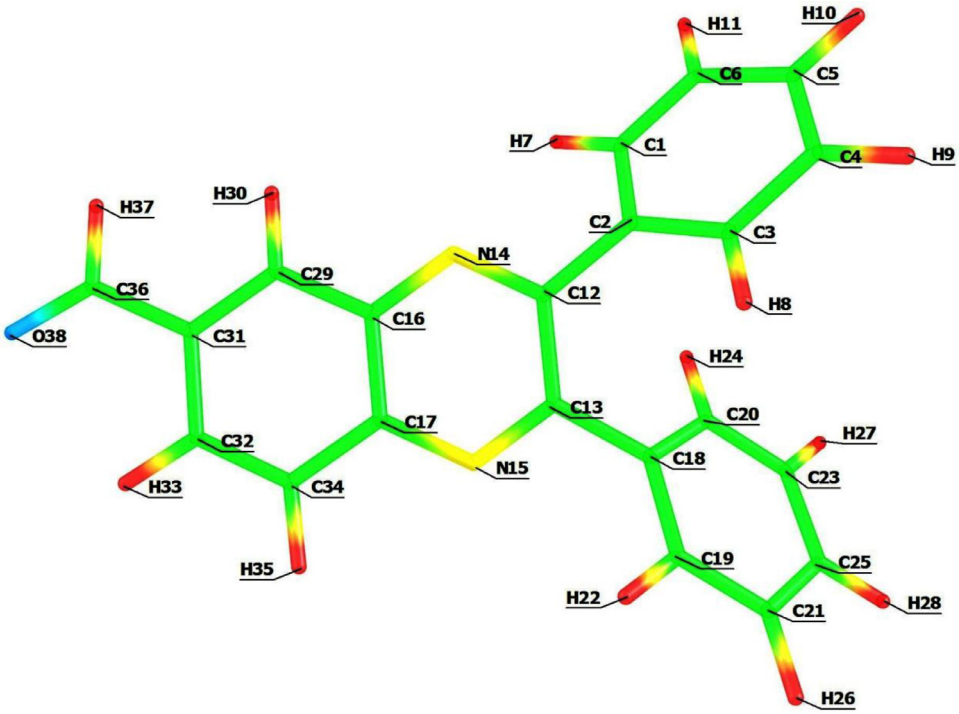

Fig. 10. NMR graphical representation of molecule **DPQC.**

ability ($\Delta\alpha$) is computed using the B3LYP/6–311G++ (d,p) basis set from Gaussian 09 W [62]. The μ, α, and β quantities in conditions of x, y, and z components of **DPQC** and **MDBD** were listed in Tables S10 and S11 (Supporting Information). Hyperpolarizability is extremely sensitive to the basic positions and levels employed by theoretical methods [63,64]. Urea is commonly used to investigate the properties of an NLO compound. Thus, the most frequently used threshold material, urea, was employed. The computed investigated molecule for the first order hyperpolarizability values is 6.734×10^{-30} esu for the DPQC molecule and 5.800×10^{-30} esu for the MDBD molecule. These hyperpolarizability values are much greater and more significant than the value of urea ($\beta o = 0.372 \times 10^{-30}$esu) [65]. The total dipole moment of the DPQC value of (μ=4.5504D) and MDBD value of (μ=1.3886D). These molecules dipole moments are also larger than the value of urea (μ=0.988D) [66]. Hence, DPQC and MDBD molecules have exhibited superior NLO properties.

3.9. (^{13}C and ^{1}H) nuclear magnetic resonance spectral data

NMR spectroscopy is a potent method for structural studies of chemical compounds [67,68]. The experimental ^{13}C and ^{1}H NMR, spectra in $CDCl_3$ solvent of the title compound **DPQC** compound was shown in Figs. S7 and S8 of the (Supporting Information) and **MDBD** compound were depicted in Figs. S9 and S10 of the (Supporting Information). The theoretical NMR spectra of the title compounds are recreated by using DFT/B3LYP method and 6–311G++(d,p) as basis set.

The slight variation achieved amongst calculated DFT/B3LYP and experimental spectra values are due to the solvent used. The **DPQC and MDBD** title compounds of ^{13}C NMR Chemical Shifts, Absolute Shielding tetramethylsilane (TMS) values are 182.4656 and 199.9853 with 31.8221 and 32.5976 (TMS) values for ^{1}H NMR spectra. As can be observed from Tables S12 and S13 (Supporting Information), the calculated ^{1}H and ^{13}C chemical shift results for DPQC and MDBD (DFT/B3LYP) values have matched the experimental data. To generate comparability with experimental observations, a correlation graph of the title compounds DPQC and MDBD have shown in Figs. S11 to S14 (Supporting Information), which gives supported to the calculations. As demonstrated from the graph, the correlation coefficient (CC) R^2 values of 0.97578 in (^{13}C NMR), 0.9788 in (^{1}H NMR) for DPQC, and (CC) R^2 values of 0.9949 in (^{13}C NMR), 0.9729 in (^{1}H NMR) for MDBD spectra. The simulated chemical shift (DFT) values are generally closed with the experimental spectra. The DFT/B3LYP/6–311G++(d,p) ^{1}H and ^{13}C NMR graphical representation of molecules DPQC and MDBD were shown in Fig. 10 and Fig. 11.

The Aromatic ring protons have a chemical shift in the region of 6.5–8.0 ppm, and also provide downfield signals in ^{1}H NMR spectra [69,70]. In our title molecule, **DPQC** proton ^{1}H NMR spectrum is observed multiplet (Ar-H) signals from the chemical shift values at δ 7.331, 7.261, 7.336, and 7.263 ppm for protons H8, H9, H26, and H27 were located in the benzene group, δ 7.485, 7.488, 7.495, 7.478, 7.474, and 7.486 ppm for protons H10, H11, H22, H26, H28, and H35 are observed in the multiplet signals of aromatic hydrogen (Ar-H), which are located in the quinoxaline group. The doublet signal detected at δ 8.191 and 8.185 ppm for protons H7 and H30 refer to the existence of (Ar-H), which are located in the quinoxaline group. The singlet signal found at δ 8.57 ppm for proton H33 indicates (Ar-H), which is presented in the quinoxaline group. Finally, one singlet signal determined at δ 10.195 ppm for proton H37 shows the appearance of aldehyde proton in the quinoxaline group in Table S12. The root-mean-square deviation (RMSD) ppm observed between experimental and calculated values are very low excepting the H7 atom, the proton ^{1}H signals at δ 7.263 to 10.195 ppm. Calculated ^{1}H NMR chemical shift for the atoms H9, H10, and H33 shows a superior agreement with the experimental spectrum.

The NMR spectrum of carbon-13 range of chemical shift for organic molecules is illustrated as generally >100 ppm [71]. The **DPQC** title compound indicated a peak chemical shift values at δ 126.77 ppm for (Ar-C) carbon C4 found in the quinoxaline group, δ 128.41 and 129.81 ppm for (Ar-C) carbon C32 and C34 are indicated with the benzil group. At δ 129.32, 129.41, 129.47, 130.46,

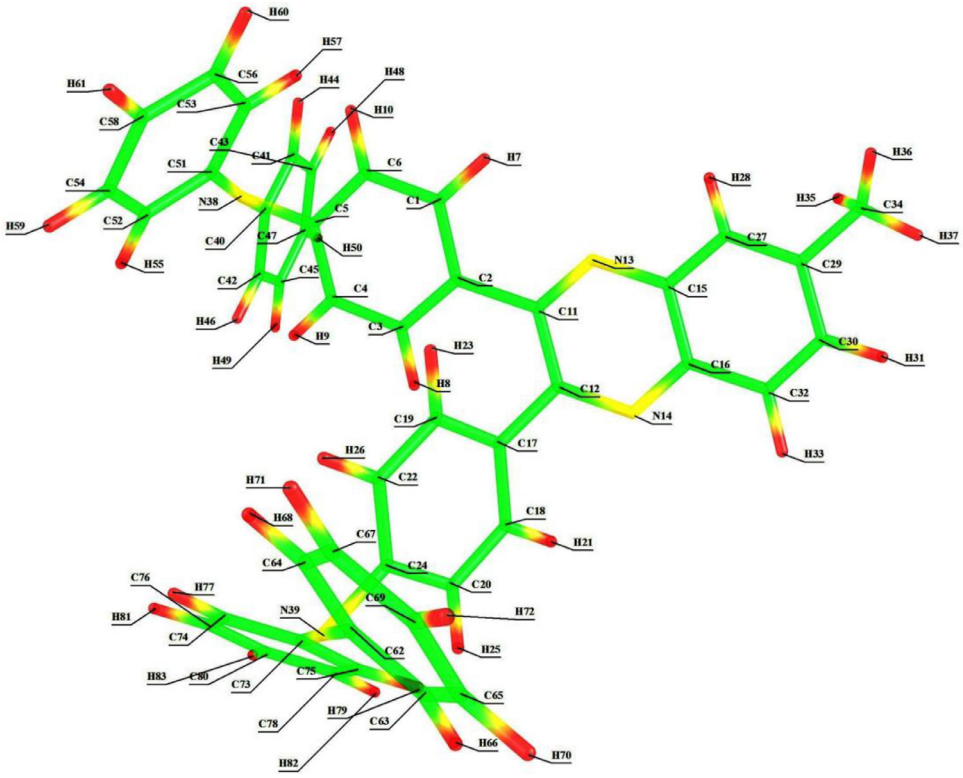

Fig. 11. NMR graphical representation of molecule **MDBD.**

134.76, 137.06, 138.46, 144.22, 154.78, and 155.60 ppm for (Ar-C) carbon C6, C21, C5, C25, C1, C23, C3, C2, C12, and C13 are found in the quinoxaline group. Finally, the peak at δ191.36 ppm for (aldehyde carbon) C36 was placed in the quinoxaline group shown in Table S12. The RMSD ppm observed between experimental and calculated values are very low excepting C12 atom, the carbon ^{13}C signals were presented at δ 126.32 to 191.36 ppm. Calculated ^{13}C NMR chemical shift for the atoms C2, C23, and C36 shows a greater concord with the experimental spectrum.

The title molecule **MDBD** proton ^{1}H NMR spectrum for the chemical shift values at δ 2.50 ppm for proton H35, shows the presence of methyl (-CH_3) protons in the quinoxaline group. The multiplet signals observed at δ 6.936 ppm for proton H8 and δ 6.966 ppm for proton H23, doublet signal observed at δ 7.098 ppm for proton H72 and δ 7.101 ppm for proton H83, and the other multiplet signals observed at δ 7.225 ppm for proton H61 and δ 7.312 ppm for proton H81 which indicates the presence (Ar-H) of triphenylamines. The doublet of doublet signal was observed at δ 7.584 ppm for proton H77 and δ 7.602 ppm for proton H46, doublet signal observed at δ 7.907 ppm for proton H26 and δ 7.911 ppm for proton H28, and doublet signal observed at δ 8.285 ppm for proton H66 and δ 8.301 ppm for proton H44, indicates the (Ar-H) existence of 6-methylquinoxaline. Finally, the doublet signal observed at δ 8.033 ppm for proton H68 and δ 8.047 ppm for proton H49 denotes the presence of the (Ar-H) triphenylamine group shown in Table S13. The RMSD ppm observed between experimental and calculated values are very low excepting the H23 atom, the proton ^{1}H signals were presented at 6.936 to 8.301 ppm. Calculated ^{1}H NMR chemical shift for the atoms H28, H61, and H72 shows a greater concord with the experimental spectrum.

A chemical shift peak at δ 21.686 ppm for carbon C34 of the title molecule **MDBD** was demonstrated the Methyl (-CH_3) carbon presented in the quinoxaline group of the carbon-13 NMR spectrum. The peaks detected at δ 122.905, 124.879, 126.271, 126.361, 129.799, 129.051, 131.628, 145.428, 147.068 ppm signals for (Ar-C) carbon C80, C69, C58, C47, C56, C54, C41, C29, and C20, which are the presence of triphenylamine. In addition, (^{13}C) NMR peaks at δ 128.861, 132.414, 140.114, 140.802, 141.247, 153.528, 154.228 ppm for (Ar-C) carbon C74, C43, C22, C53, C15, C12, and C11, which are found to indicating the presence (Ar-C) of 6-methylquinoxalin group shown in Table S13. The RMSD ppm observed between experimental and calculated values are very low excepting C34 atom, the carbon ^{13}C signals were presented at δ 126.32 to 191.36 ppm. Calculated ^{13}C NMR chemical shift for the atoms C20, C41, and C74 shows a good deal with the experimental spectrum. The aforementioned spectrum data is very well aligned by both experimental and DFT calculation with the structures of the new quinoxaline DPQC and MDBD derivatives.

3.10. Mass spectrum

The mass spectrum range of synthesized the novel quinoxaline derivatives with its molecular ion peak observed at *m/z* 311.40 for DPQC and *m/z* 631.73 for MDBD compounds are owing to the existence of (MH+), which coincides with the molecular mass, their (*m/z*) scale ranges observed at 200–2000 presented in Figs. S15 and S16 (Supporting Information). The observed molecular ion peaks in the spectra match the predicted molecular structures of the title compound perfectly. The spectrophotometers were run in positive scan mode.

3.11. Biological evaluations

3.11.1. Antibacterial activity

The title compounds **DPQC and MDBD** from formulated powder showed broad-spectrum antibacterial activity against Gram (+) and Gram (−) bacteria using streptomycin as a positive control. The **DPQC** molecule showed potent bactericidal activity with a maximum of (17.7±1.0 mm) at 2.5 µg/mL against *Staphlococcus aureus*

Table 2
Antibacterial activity of **DPQC** against Gram-positive and Gram-negative bacteria.

Organisms	Streptomycin (mm)	Antibacterial activity (mm)				
		0.5(μg/ml)	1(μg/ml)	1.5(μg/ml)	2(μg/ml)	2.5(μg/ml)
Staphylococcus aureus (MTTC 3615)	20.1±1.0	12.3±0.5	13.2±0.5	14.4±0.5	15.5±1.1	17.7±1.0
Enterococcus faecalis (MTCC 439)	19.8±0.5	11.3±0.5	11.9±1.0	12.6±1.0	13.3±0.5	14.8±1.1
Y. enterocolitica (MTCC 840)	19.7±0.5	10.3±0.5	11.0±0.5	12.7±0.5	13.6±1.0	15.6±1.0
Proteus mirabilis (MTCC 1771)	20.1±0.5	12.3±0.5	13.5±0.5	14.5±1.0	15.3±1.0	17.5±1.0

Table 3
Antibacterial activity of **MDBD** against Gram-positive and Gram-negative bacteria.

Bacteria	Streptomycin (mm)	Antibacterial activity (mm)				
		0.5(μg/ml)	1(μg/ml)	1.5(μg/ml)	2(μg/ml)	2.5(μg/ml)
Staphylococcus aureus (MTTC 3615)	21.6±0.5	15.6±0.5	14.3±0.5	15.3±0.5	17.6±0.5	18.6±1.0
Enterococcus faecalis (MTCC 439)	21.4±0.5	16.6±0.5	17.3±1.1	17.9±1.0	18.3±0.5	19.0±1.0
Y. enterocolitica (MTCC 840)	22.3±0.5	17.1±1.0	17.8±0.5	18.0±1.0	18.8±1.0	19.5±1.0
Proteus mirabilis (MTCC 1771)	21.0±0.5	15.4±0.5	15.9±1.1	17.7±1.0	18.8±0.5	19.1±1.1

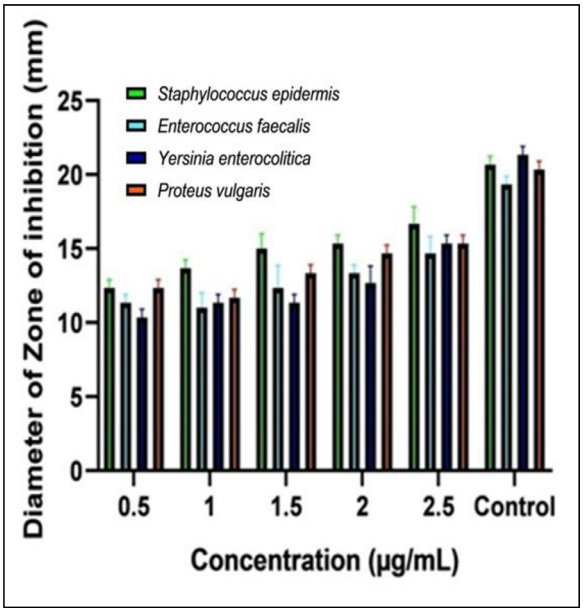

Fig. 12. Antibacterial activity of DPQC against Gram-positive and Gram-negative bacteria.

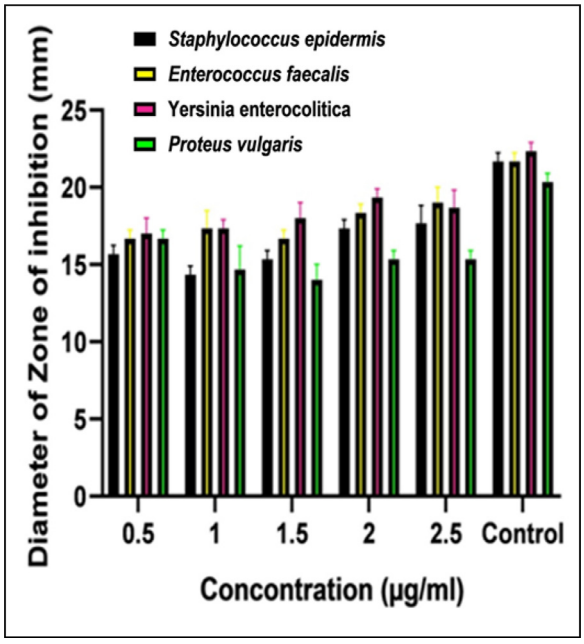

Fig. 13. Antibacterial activity of **MDBD** against Gram-positive and Gram-negative bacteria.

(MTCC 3615) and minimum zone of inhibition of (10.3±0.5 mm) on *Y. enterocolitica* (MTCC 840) (Table 2 and Fig. 12) at 0.5 μg/mL respectively. The **MDBD** molecule showed potent bactericidal activity with a maximum of (19.5±1.0 mm) at 2.5 μg/mL against *Y. enterocolitica* (MTCC 840) and minimum zone of inhibition of (14.3±0.5 mm) on *Staphylococcus aureus* (MTCC 3615) (Table 3 and Fig. 13) at 1 μg/mL respectively.

Yokoyama A. and coworkers examined the antibacterial activities of 2,3-Bis(bromomethyl)quinoxaline derivatives, and reported that only 2,3-Bis(bromomethyl)-6-ethoxycarbonylquinoxaline molecule showed activities against Gram-negative bacteria (Escherichia coli, Pseudomonas aerugianosa, and Serratia marcescens) [72]. As a result, it is possible that it is due to an increase in the length of the alkyl chain. However, since the DPQC molecule aldehyde (-CHO) group has no action against Gram (-) bacteria, the MDBD molecule's activity against Gram (-) bacteria can be explained by the source of the offerings of the incorporated aromatic ring and ($-CH_3$) groups [73,74], which we know should increase the lipophilicity of the molecules [75]. This increase in lipophilicity would improve their permeability through the microbial cell wall, leading to increased activity. Because of the presence of the triphenylamine group [76–78], the MDBD molecule may be regarded as an analogue of triphenylamine (a recognised antibacterial).

3.11.2. In vitro *antioxidant activity (H_2O_2 and dpph radical scavenging activity)*

According to a pharmaceutical technique, the H_2O_2 scavenging test was estimated [23]. The findings of the antioxidant research (H_2O_2) showed that the produced MDBD synthesized compound may be a good source of the activity of hydroxyl radical scavenging.

Hydroxyl radicals ($OH^{\cdot}$) are short-lived species possessing a high affinity for other molecules. OH is a strong oxidizing agent that can react at a high rate with the majority of lipids, amino acids, sugars, and metals. Because OH is identified as the primary reactive radicals in biological systems, it interacts with nearby molecules at the point of origin. The substance damages the cell membrane's polyunsaturated fatty acid moieties. Hydroxyl radicals are produced in several ways. OH, scavenging activity of synthe-

Table 4
Antioxidant activity of synthesized quinoxaline derivatives.

Sample Name	Control	Test (1 mg/mL)	H_2O_2 Scavenging (%)
DPQC	3.8	3.1	18.42
MDBD	3.8	1.36	64.21

Table 5
Antioxidant activity of test compounds 2,3-Diphenylquinoxaline derivatives **(DPQC** and **MDBD),** measured by DPPH assay.

Concentration (µg/ml)	% of Inhibition	Standard Drug	
	DPQC	MDBD	D - Ascorbic acid
100	17.99	19.01	47.37
200	30.94	32.31	55.32
300	40.01	40.39	69.43
400	52.32	54.73	86.45
500	59.76	67.48	90.89

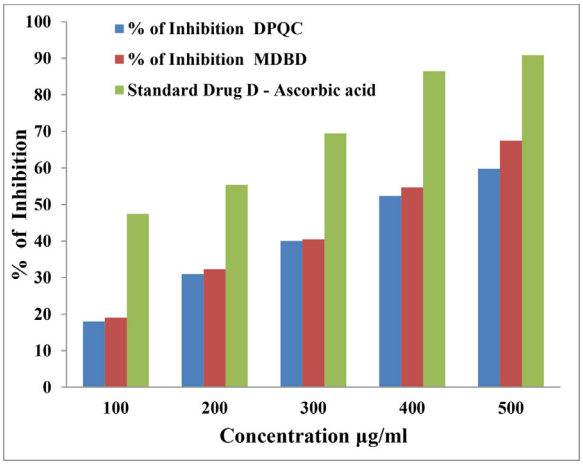

Fig. 14. *In vitro* DPPH radical scavenging activity of test compounds **DPQC** and **MDBD**.

sized compounds determined that MDBD possessed the greatest antioxidant capacity compared to DPQC. *In vitro*, antioxidant activities were demonstrated in Table 4.

The synthesized compounds **(DPQC and MDBD)** were evaluated for their capability to scavenge the free radicals formation which was measured by the DPPH assay method [79,80]. The antioxidant activities of the synthesized compound were shown in Table 5. The D-ascorbic acid (Vitamin C) was utilized as a standard antioxidant. The IC_{50} values for each compound were calculated and found that all the antioxidant tested compounds 2,3-Diphenylquinoxaline derivatives such as DPQC and MDBD possess IC_{50} values in close ranges from 365.4303–382.2765 µg/mL. There was not much difference between these compounds in scavenging the free radical results Fig. S17 (Supporting Information). When compared to the standards, all the compounds exhibited activity of free radical scavenging, particularly the compound MDBD showed strong antioxidant activity (67.48 %) at the concentration of 500 µg/mL followed by compound DPQC showed (59.76 %) and D-ascorbic acid (Vitamin C) showed the activity of 90.89 % of free radical scavenging concentration at 500 µg/mL (Table 5). All the compounds possessed good radical scavenging activity (Fig. 14).

The plausible mechanism for the antioxidant activity of MDBD against DPPH is exhibited in Fig. 15. Of all the synthesized compounds DPQC and MDBD, the compound MDBD exhibited excellent, explicit from Fig. 15. According to the mechanism, we have proved that the triphenylamine group participates in the antioxidant process on the DPPH assay. A probe through the literature reveals [81,82] that DPPH can be quenched by hydrogen atom transfer (HAT), electron transfer (ET), or a combination of both. In the compound, MDBD both HAT and electron transfers (ET) mechanisms were involved.

The electron transfer mechanism consists of forming a complex of an aminium cation radical and DPPH anion. As per the HAT mechanism, the removal of hydrogen radicals from both MDBD would reflect their antioxidant activities.

Table 6
Anticancer activity of synthesized **DPQC** and **MDBD** test compounds measured by MTT assay and (HepG2) liver cancer cell line.

% of Concentration (µg/ml)	% of cell viability	
	DPQC	MDBD
15.75	81.8	89.2
31.25	78.4	87.1
62.5	76.6	85.2
125	58.2	83.3
250	45.3	81.2
Control (HepG2) cell-line	100	100

3.11.3. In vitro *anticancer activity*

Most of the quinoxaline derivatives have been observed to be successful *in vitro* cytotoxic compounds against a human liver tumour cell line [83,84]. In this study, we analysed all the synthesized new **DPQC and MDBD** compounds for their anticancer activity. The (HepG2) liver cancer cell lines-Controls image was represented in Fig. 16**a**. amongst the two compounds studied the compound MDBD showed the anticancer activity at the lowest concentration of 125 µg/mL (Table 6 and Fig. 16**b**). This compound reduced the cell viability to 83.3 % respectively and cell viability was much more decreased to 81.2 % respectively at 250 µg/mL. The HepG2 - liver cancer cells were tested at concentrations from 15.75 µg/mL to 250 µg/mL. The compound DPQC showed potent anticancer activity only at a higher concentration of 250 µg/mL. The resultant (HepG2) cell line image and graphical representations of DPQC were shown in Fig. 16**c**. The anticancer activities of synthesized DPQC and MDBD test compounds measured by MTT assay and (HepG2) liver cancer cell line images were given in Fig. 17.

3.12. In silico section

3.12.1. Molecular docking studies

The compounds studied, **DPQC and MDBD** showed significant *in vitro* anticancer activity. Hence, these compounds were further investigated *in silico* molecular docking analysis against 3F66 (c-Met-kinase; a hepatocyte growth factor) protein target. Receptor tyrosine kinases (RTKs) are interesting pharmacological targets important for developing tumours and controlling the many routes of signal transduction inside the cell. The molecular profile of patients, particularly based on the molecular pathways associated with cancer start and development, is created according to new treatments. The c-metal acts on hepatocyte growth factor (HGF) and the reshaping, migration, morphogenesis, cell development, differentiation, and angiogenesis of the epithelial tissue [85–87]. Deregulated activation of the c-Met-signalling pathway through multiple mechanisms like activation, mutation, gene amplification, and heterodimerization has been reported to correlate with high tumour grade and the lower rate of survival in most cancers [88]. Moreover, in 2011, c-Met-was found as a marker of pancreatic cancer stem cells, which made it a suitable therapeutic target for cancer treatment [89]. Applying the scoring functions to the AutoDock Vina software [90]. The 3F66 resolution was 1.4 Å [31] for x-ray

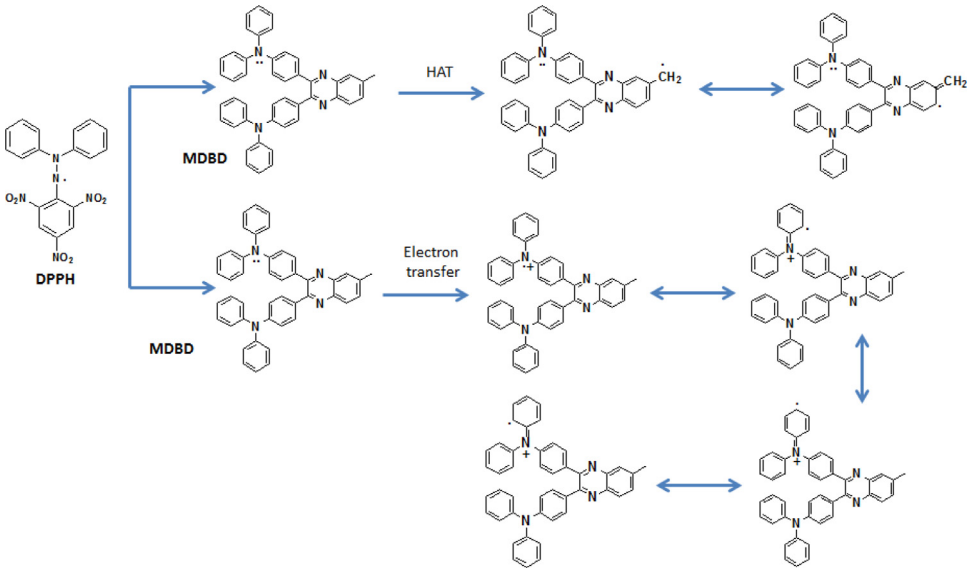

Fig. 15. Plausible antioxidant mechanism of compound **MDBD** against DPPH radical.

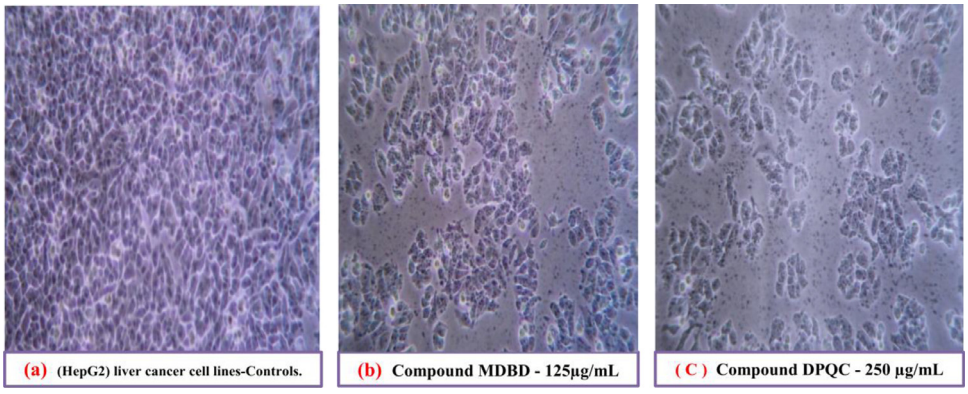

Fig. 16. **(a)** (HepG2) liver cancer cell lines-Controls. **(b)** (HepG2) liver cancer cell lines image **MDBD.** **(c)** (HepG2) liver cancer cell lines image **DPQC.**

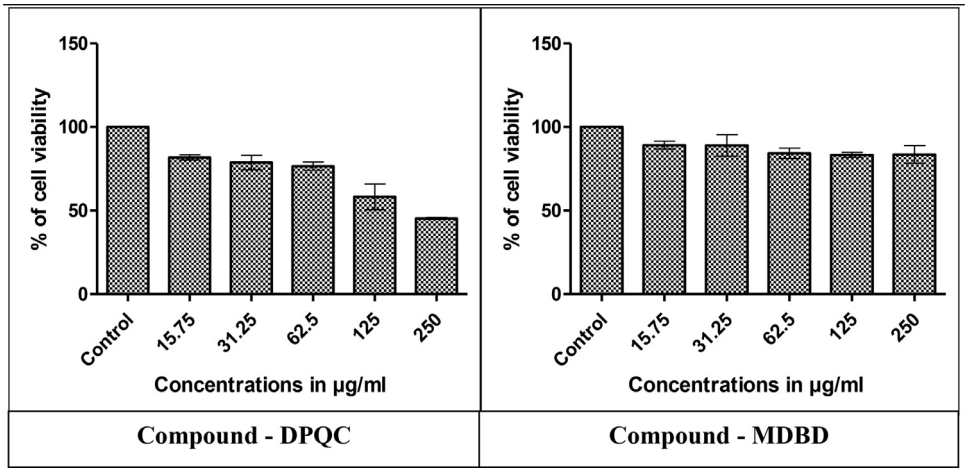

Fig. 17. Anticancer activities of synthesized **DPQC** and **MDBD** test compounds measured by MTT assay and (HepG2) liver cancer cell line.

diffraction. The Root Mean Square Deviation (RMSD) should be approx. 2 Å for a molecular docking process, which value is recognized to be trustworthy for docking [91].

The Human c-Met-Kinase receptor has been presented with the binding affinity energy values and RMSD values as per (rmsdl.b and rmsdu.b). Furthermore, the inhibition constants for all compounds were computed and recorded using Ki=exp ($\Delta G/RT$), where = ΔG, R and Tare docking energy, gas constant (1.9872036×10^{-3} kcal/mol), and room temperatures (298.15 K), were computed and recorded. Let's examine each docking method

Table 7
The ligand- receptor residue interaction between **DPQC, MDBD, and Standard drug Trivatinib** with **3F66** protein.

S.NO	Pub chem. Id	Ligand Name	Residue Interaction	Type of bond	Distance (Å)
1	3F66	DPQC	A: ASN1175: NH-:UNK0:O24	Hydrogen	2.09
			A: ASP1180: OD2-:UNK0	π-Anion Electrostatic	3.74
			A: ASP1180: OD2-:UNK0	π-Anion Electrostatic	3.92
			A: PHE1216-:UNK0	π- π- Stacked Hydrophobic	3.87
			A: PHE1216-:UNK0	π- π- Stacked Hydrophobic	4.03
			A: ARG1086:NH -:UNK0:N6	Hydrogen	2.91
2	3F66	MDBD	A: MET1211: SD-:UNK0	π-Sulfur	5.68
			A: MET1211: SD-:UNK0	π-Sulfur	5.08
			: UNK0-A: VAL1092	π-Alkyl Hydrophobic	5.68
			: UNK0-A: ALA1226	π-Alkyl Hydrophobic	5.14
			: UNK0-A: ALA1108	π-Alkyl Hydrophobic	4.39
			: UNK0-A: MET1211	π-Alkyl Hydrophobic	5.13
3	3F66	Standard Drug Trivatinib (Pbchem ID – 11,494,412)	A: LYS1248:H -:UNK0:O1	Hydrogen	2.2
			A: ASN1288:C -:UNK0:O1	Hydrogen	3.53
			: UNK0:H-A: SER1236:OG	Hydrogen	2.91
			A: LYS1248: NZ-:UNK0	π-Cation Electrostatic	4.12
			A: LYS1248: NZ-:UNK0	π-Cation Electrostatic	3.35
			A: LYS1248-:UNK0	Alkyl Hydrophobic	4.8
			A: PRO1283-:UNK0	Alkyl Hydrophobic	5.47

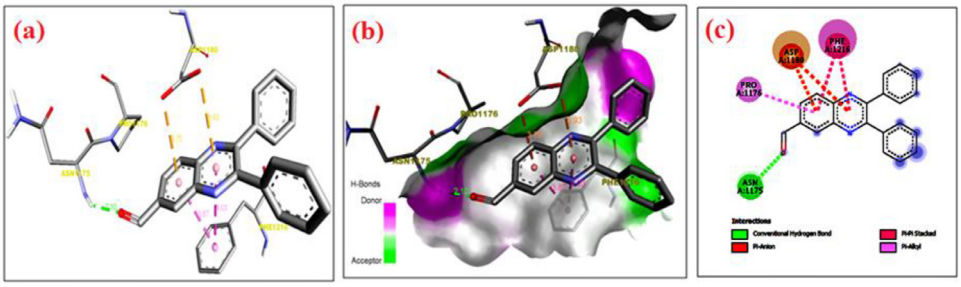

Fig. 18. The molecular docking results of the title compound **(DPQC) (a)** Hydrogen bond Interaction of **DPQC** ligand with **3F66** protein **(b)** Hydrogen bond Receptor-side surface Interaction of **DPQC** ligand with **3F66** protein. **(c)** 2D-Hydrogen bond Interaction representation of **DPQC** ligand with **3F66** protein.

for the proteins utilized one by one. The Inhibition constant (ki) describes the interaction between the ligand and an enzyme substance, whereas, ki measures the ligand-binding affinity to the protein. If (ki) is lower, less medication is essential to inhibit the enzyme's activity. Additionally, the (ki) value is found to be confirmed if a medication is going to block an enzyme and consequence in a clinically relevant specific drug with a substrate for the enzyme [92–94]. The binding affinity and inhibition constant of (ki) of all resulting ligands are presented in Table S14 (Supporting Information). The results indicate, with residual interactions, types of bond, and bond lengths, that all DPQC, MDBD, and Standard Drug Tivantinib ligands could strongly occupy the active site of 3F66 was shown in Table 7 In this study, we have depicted intermolecular interactions of different DPQC, MDBD, and Tivantinib ligands with the Human c-Met-Kinase (PDB code: 3F66) protein, respectively.

The ligand **DPQC** (within 3F66) molecular docking ligand-receptor hydrogen bond interactions, Receptor side hydrogen bond interactions, and their 2D-ligand-receptor hydrogen bond interaction graphical representation were given in (Fig. 18a, b, and c) with a binding energy value of -7.9 (kcal/mol), 1.59526 µM inhibition constant (ki) and also presented one hydrogen bond interaction between (ASN1175: NH amino acid residue and O24 atom; bond angle of 2.09 Å), respectively; two π-anion electrostatic interactions were formed between the quinoxaline group with (Two ASP1180: OD2 amino acid residues; bond angle values are 3.74 and 3.92 Å), respectively; two π- π stacked hydrophobic interactions were formed between the quinoxaline group with (Two PHE1216 amino acid residues; bond angle values are 3.87 and 4.03 Å). Fig. 18**a** shows clearly that the hydrogen bond is denoted (Green colour), π-anion electrostatic interactions are shown (Dark Pink colour), and finally, π-π stacked hydrophobic interactions have been shown (yellow colour).

The ligand **MDBD** (within 3F66) molecular docking ligand-receptor hydrogen bond interactions, Receptor side hydrogen bond interactions, and their 2D-ligand-receptor hydrogen bond interaction graphical representation were given in (Fig. 19**a, b**, and **c**) with a binding energy value of -10.8 (kcal/mol), 0.01187 µM inhibition constant (ki) and also presented one hydrogen bond interaction between (ARG1086:NH amino acid residue and N6 atom; bond angle of 2.91 Å), respectively; two π-Sulfur interactions were formed between the triphenylamine group with (Two MET1211: SD amino acid residues; bond angle values are 5.08 and 5.68 Å), respectively; four π-Alkyl Hydrophobic interactions were formed between the triphenylamine group with (Four VAL1092/ALA1226/ALA168/MET1211 amino acid residues; bond angle values are 5.68, 5.14, 4.39, and 5.13 Å). Fig. 19**a** shows clearly that the hydrogen bond is denoted (green colour), π-Sulfur interactions are shown (yellow colour), and finally, π- Alkyl hydrophobic interactions have been shown (pink colour).

In our study, Tivantinib [95] ligand was selected as a standard drug because, generally, Tivantinib is an orally bioavailable small molecule inhibitor of c-Met-with potential antineoplastic activity. The c-Met-inhibitor ARQ 197 binds to the c-Met-protein and disrupts c-Met-signal transduction pathways, inducing cell death in tumour cells over expressing c-Met-protein or expressing the constitutively activated c-Met-protein. The ligand Tivantinib (within 3F66) molecular docking ligand-receptor hydrogen bond interactions, Receptor side hydrogen bond interactions, and their 2D-ligand-receptor hydrogen bond interaction graphical representation

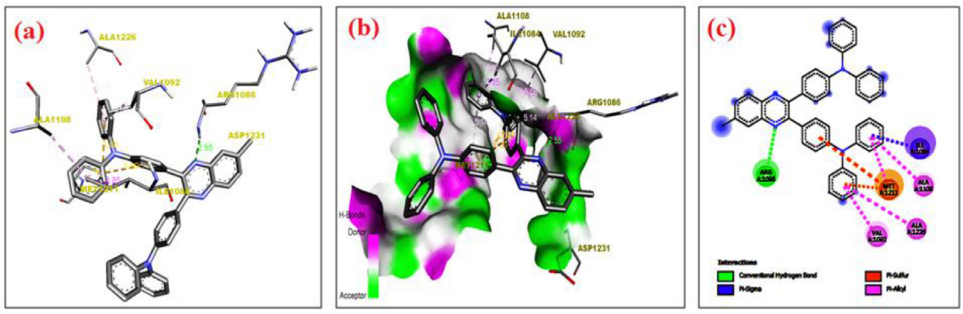

Fig. 19. The molecular docking results of the title compound (**MDBD**) **(a)** Hydrogen bond Interaction of **MDBD** ligand with **3F66** protein **(b)** Hydrogen bond Receptor-side surface Interaction of **MDBD** ligand with **3F66** protein. **(c)** 2D-Hydrogen bond Interaction representation of **MDBD** ligand with **3F66** protein.

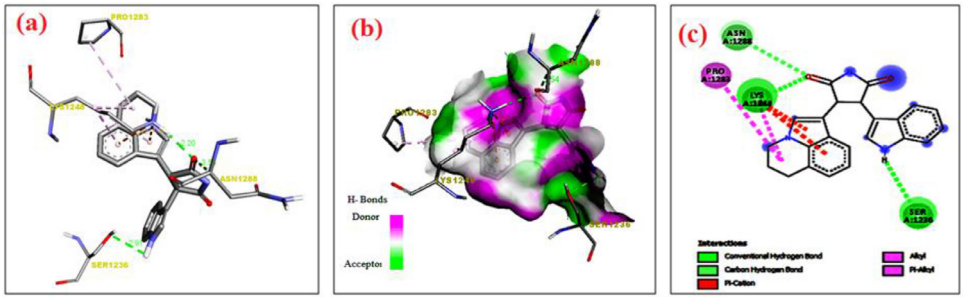

Fig. 20. The molecular docking results of the title compound (**Standard Drug Trivatinib**) **(a)** Hydrogen bond Interaction of **Trivatinib** ligand with 3F66 protein **(b)** Hydrogen bond Receptor-side surface Interaction of **Trivatinib** ligand with 3F66 protein. **(c)** 2D-Hydrogen bond Interaction representation of **Trivatinib** ligand with 3F66 protein.

were given in (Figs. 20**a, b**, and **c**) with a binding energy value of -8.3 (kcal/mol), 0.81153 μM inhibition constant (ki) and also presented two hydrogen bond interactions between carbonyl (C=O) functional groups which were presented in the pyrrolidine ring with (LYS1248:H amino acid residue and O1 atom; bond angle of 2.20 Å), (ASN1288:C amino acid residue and O1 atom; bond angle of 3.53 Å), and one hydrogen bond interaction between the indole group with (SER1236:OG amino acid residue and H atom; bond angle of 2.91 Å), respectively; two π-Cation Electrostatic interactions were formed between the 5,6-dihydro-4H-pyrrolo[3,2,1-ij]quinoline group with (Two LYS1248: NZ amino acid residues; bond angle values are 4.12 and 3.35 Å), respectively; two alkyl hydrophobic interactions were formed between the 5,6-dihydro-4H-pyrrolo[3,2,1-ij]quinoline group with (Two LYS1248 amino acid residues; bond angle values are 4.80, and 5.47 Å). Fig. 20**a** shows clearly that the hydrogen bond is denoted (Green colour), π-Cation Electrostatic interactions have been shown (pink colour), and finally, alkyl hydrophobic interactions have been shown (pink colour). In this molecular docking study, the newly synthesized DPQC ligand has shown the best binding energy, as well as good inhibition constant (ki) values, with these values being very close to the standard drug, tivantinib. Human c-Met-Kinase in complex with quinoxaline inhibitor (PDB code: 3F66; chosen active site A) protein with the target compound MDBD, which has shown a significant binding interaction energy value of-10.8 (kcal/mo) compared to the known standard drug tivantinib-8.3 (kcal/mol). The binding interaction energy value of DPQC was -7.9 (kcal/mol), which was nearly equal to tivantinib.

- ➢ The Residue Interaction column (UNK0) Symbol is described as ligand side with its functional groups such as O, S, N…..ect.
- ➢ A: is indicates as a protein chain.

4. Conclusions

The present work describes a series of novel **DPQC** and **MDBD** possessing quinoxaline moiety containing compounds that have been synthesized by direct condensation reaction, and their various physical and spectroscopic techniques, particularly, FT-IR, UV-Visible spectroscopy, ^{1}H, and ^{13}C NMR, ESI-Mass spectrum, and elemental (CHNS/O) analysis have been carried out. The structural geometrical parameters, vibrational, electronic, HOMO-LUMO, Mulliken population analysis, and Molecular electrostatic potentials (MEPs) were carried out by the DFT calculations on the B3LYP/6–311G++(d,p) basis set. An excellent agreement between experimental and calculated wavenumbers and all observed wavenumbers have been assigned. The Frontier Molecular Orbitals (FMOs) analysis of (HOMO-LUMO) energy (Gap (eV) = 3.8448) for the DPQC molecule and (Gap (eV) = 3.1212) for the MDBD molecule. In DFT, the electron affinity (A) study of DPQC and MDBD showed a low electron affinity HOMO-LUMO value of 2.4165 (eV) and 1.7226 (eV). The NLO investigations confirm that the **DPQC and MDBD** compounds are excellent NLO materials. Furthermore, in the biological evaluations studies, the antibacterial activities have been done for the novel **DPQC and MDBD** compounds against Gram (+) and Gram (−) bacteria using the disc diffusion technique and the result discovered that the MDBD compound showed important antibacterial activity against Gram (+) and Gram (−) bacteria owing to the existence of triphenylamine group. The compound MDBD showed a strong hydrogen peroxide (H_2O_2) and DPPH radical scavenging antioxidant activities and revealed potent anticancer activity against human liver cancer (HepG2) cell lines. In molecular docking investigation **MDBD** ligand, which has shown the best binding energy value of -10.8 (kcal/mol), and a 0.01187 μM inhibition constant (ki) against the Human c-Met-Kinase (PDB code: 3F66; chosen active site A) involved amino acids such as A: ARG1086, A: MET1211, A: VAL1092, A: ALA1226, A: ALA1108, A: MET1211. Hence, it has given superior binding energy and very powerful inhibition constant (ki) values compared to both DPQC and trivatinib ligands. Hence, the MDBD ligand will be a medication needed to inhibit the Human c-Met-Kinase (PDB code: 3F66) protein. The synthesized quinoxaline derivatives thus have certain biochemical potential and might be more likely to create medicines associated with diverse microbial, fungal and viral illnesses.

Credit author statement

J. Irshad Ahamed: Conceptualization, Supervision, Spectral characterizations, *In vitro* studies, analysing results, Writing - review & editing.

G.R. Ramkumaar: Methodology and computational analysis studies.

P. Kamalarajan, K. Narendran, and M. F. Valan: Formal analysis, Methodology.

S. Bharathi: Investigation Visualization.

B. Venkatadri: Antibacterial studies

T. Sundareswaran and T.A Sundaravadivel: *In Silico* analysis work.

Declaration of Competing Interest

I certify that ALL of the following statements are correct.

The manuscript represents valid work.

Neither this manuscript nor one with substantially similar content under my authorship has been published or is being considered for publication elsewhere (except as described in the manuscript submission).

We confirm that the manuscript has been read and approved by all named authors and that there are no other persons who satisfied the criteria for authorship but are not listed. We further confirm that the order of the authors listed in the manuscript has been approved by all of us.

Scientific, ethical and legal responsibility of the article belongs to us as the authors. We are responsible for the ideas, comments and accuracy of references in the article.

We wish to confirm that there are no known conflicts of interest associated with this publication and there has been no significant financial support for this work that could have influenced its outcome.

Conception and planning of the work that led to the manuscript or acquisition, analysis and interpretation of the data.

We understand that the Corresponding Author is the sole contact for the Editorial process. He is responsible for communicating with the other authors about progress, submissions of revisions and final approval of proofs.

Acknowledgements

The authors are delighted to thank C. Kandaswami Naidu College for Men, Department of chemistry (SHIFT – II) and LIFE (Loyola Institute of Frontier Energy) for supporting this study by providing us with laboratory facilities, instrumental facilities and infrastructural facilities. Also, thanks to the Plant Biology & Biotechnology Department, Loyola College (Autonomous), for providing the laboratory facilities for *in vitro* studies and to the Department of Chemistry, Saveetha Engineering College, Thandalam, for supporting this work. I also thank T. Sundareswaran and T.A Sundaravadivel, who helped perform the *in silico* molecular docking studies.

Supplementary materials

Supplementary material associated with this article can be found, in the online version, at doi:10.1016/j.molstruc.2021.131418.

References

[1] V.N. Toan, N.D. Thanh, N.M. Tri, Arab. J. Chem. 14 (2021) 103053.
[2] J.A. Pereira, A.M. Pessoa, M.N.D. Cordeiro, R. Fernandes, C. Prudêncio, J.P. Noronha, M. Vieira, Eur. J. Med. Chem. 97 (2015) 664–672.
[3] A.C Pinheiro, T.C Mendonça Nogueira, M.VN de Souza, Anticancer Agents Med. Chem. 16 (2016) 1339–1352.
[4] N.A. Alsaif, M.A. Dahab, M.M. Alanazi, A.J. Obaidullah, A.A. Al-Mehizia, M.M. Alanazi, S. Aldawas, H.A. Mahdy, H. Elkady, Bioorg. Chem. 110 (2021) 104807.
[5] M.M. Alanazi, H.A. Mahdy, N.A. Alsaif, A.J. Obaidullah, H.M. Alkahtani, A.A. Al-Mehizia, S.M. Alsubaie, M.A. Dahab, I.H. Eissa, Bioorg. Chem. 112 (2021) 104949.
[6] S.A. Galal, A.S. Abdelsamie, S.M. Soliman, J. Mortier, G. Wolber, M.M. Ali, H. Tokuda, N. Suzuki, A. Lida, R.A. Ramadan, H.I. El Diwani, Eur. J. Med. Chem. 69 (2013) 115–124.
[7] M. Missioui, S. Mortada, W. Guerrab, G. Serdaroğlu, S. Kaya, J.T. Mague, E.M. Essassi, M.E.A. Faouzi, Y. Ramli, J. Mol. Struct. 1239 (2021) 130484.
[8] S. Koppireddi, J.R. Komsani, S. Avula, S. Pombala, S. Vasamsetti, S. Kotamraju, R. Yadla, Eur. J. Med. Chem. 66 (2013) 305–313.
[9] N.P. Desai, V. Trieu, L.Y. Hwang, R. Wu, P. Soon-Shiong, W.J. Gradishar, Anti–cancer drugs 19 (2008) 899–909.
[10] M.J. Frisch, G.W. Trucks, H.B. Schkegel, G.C. Scuseria, M.A. Robb, J.R. Cheeseman, G. Scalmani, V. Barone, B. Mennucci, G.A. Bloino, G. Zheng, J.L Sonnenberg, M. Hada, M. Ehara, K. Toyota, R. Fukuda, J. Hasegawa, M. Ishida, T. Nakajima, Y. Honda, O. Kitao, H. Nakai, T. Vreven, J.A. Montgomery, J.E. Peralta, F. Ogliaro, M. Bearpark, J.J. Heyd, E. Brothers, K.N. Kudin, V.N. Staroverov, T. Keith, R. Kobayashi, J. Normand, K. Rghavachri, A. Rendell, J.C. Burant, S.S. Iyengar, J. Tomasi, M. Cossi, N. Rega, J.M. Millam, M. Klene, J.E. Knox, J.B. Cross, V. Bakken, C. Adamo, J. Jaramillo, R. Gomperts, R.E. Stratmann, O. Yazyev, A.J. Austin, R. Cammi, C. Pomelli, J.W. Ochterski, R.L. Martin, K. Morokuma, V.G. Zakrzewski, G.A. Voth, P. Salvador, J.J. Dannenberg, S. Dapprich, A.D. Daniels, O. Farkas, J.B. Foresman, J.V. Ortiz, J. Cioslowski, D.J. Fox, Gaussian 09, Revision D.01, Gaussian Inc, Wallingford CT, 2013.
[11] J. Irshad Ahamed, M. Priya, P. Vinothkumar, K. Sathyamoorthy, P. Murali-Manohar, J. Liu, M.F. Valan, J. Mol. Struct. 1202 (2020) 127241.
[12] M.H. Jamroz, Vibrational Energy Distribution Analysis VEDA 4, 2004. Warsaw.
[13] J. Irshad Ahamed, M.F. Valan, K. Pandurengan, P. Agastian, B. Venkatadri, M.R. Rameshkumar, K. Narendran, Res. Chem. Intermed. 47 (2021) 759–794.
[14] S. Srivastava, P. Gupta, A. Sethi, R.P. Singh, J. Mol. Struct. 1117 (2016) 173–180.
[15] E. Kose, A. Atac, M. Karabacak, C. Karaca, M. Eskici, A. Karanfil, Spectrochim. Acta A. 97 (2012) 435–448.
[16] M. Karabacak, L. Sinha, Z.Cinar O.Prasad, M. Cinar, Spectrochim. Acta A 93 (2012) 33–46.
[17] B.F. Rizwana, J.C. Prasana, S. Muthu, C.S. Abraham, J. Mol. Struct. 1202 (2020) 127274.
[18] Gauss View 5.09 program Gaussian, Inc., Wallingford, CT, 06492 USA.
[19] N.M. O'Boyle, A.L. Tenderholt, K.M. Langner, J. Comp. Chem. 29 (2008) 839–845.
[20] B.R. Raajaraman, N.R. Sheela, S. Muthu, J. Mol. Struct. 1173 (2018) 583–595.
[21] R. Duchfield, J. Chem. Phys. 56 (1972) 5688–5691.
[22] K. Wolinski, J.F. Hinton, P. Pulay, J. Am. Chem. Soc. 112 (1990) 8251–8260.
[23] B. Venkatadri, A. Khusro, C. Aarti, M.R. Rameshkumar, P. Agastian, Asian. Pac. J. Trop. Biomed. 7 (2017) 782.
[24] https://www.rcsb.org/structure/3f66.
[25] G.M. Morris, D.S. Goodsell, R.S. Halliday, R. Huey, W.E. Hart, R.K. Belew, A.J. Olson, J. Computational Chemistry. 19 (1998) 1639–1662.
[26] D.S. Visualizer, Discovery Studio Visualizer, Accelrys software inc., 2005.
[27] G.N. Raju, Y. Sravani, K.N.S. Sri, B. Revathi, N. Ramarao, World J. Pharm. Pharmaceut. Sci. 4 (2015) 2019–2030.
[28] G. Bernardo, M.A. Esteves, A.M. Guerreiro, B. Gigante, J. Morgado, Opt. Mater. 31 (2008) 320–327.
[29] R.S. Mulliken, J Chem Phys 23 (1955) 1833-1840.
[30] M. Karabacak, L. Sinha, O. Prasad, A.M. Asiri, M. Cinar, V.K. Shukla, Spectrochim. Acta A. 123 (2014) 352–362.
[31] Ö. Bağlayan, M.F. Kaya, E. Güneş, M. Şenyel, J. Mol. Struct. 1122 (2016) 324–330.
[32] G. Keresztury, Raman spectroscopy: theory, in: J.M. Chalmers, P.R. Griffith (Eds.), Handbook of Vibrational spectroscopy, John Wiley & Sons, New York, 2002.
[33] A. Uppal, P. Kour, A. Kumar, Y. Khajuria, J. Mol. Struct. 1166 (2018) 218–227.
[34] G. Brahmachari, S. Das, A. Kumar, N. Misra, S. Sharma, V.K. Gupta, J.Mol.Struct 1136 (2017) 214–221.
[35] K. Subashini, S. Periandy, J.Mol.Struct 1117 (2016) 240–256.
[36] Y.Köysal H.Tanak, Y. Ünver, M. Yavuz, S. Isık, K. Sancak, Mol. Phys. 108 (2010) 127–139.
[37] D. Zhao, K.D. Doney, H. Linnartz, J. Mol. Struct. 296 (2014) 1–8.
[38] S. Sevvanthi, S. Muthu, M. Raja, J. Mol. Struct. 1173 (2018) 251–260.
[39] P.J. Brimmer, P.R. Griffiths, Appl. Spectrosc. 42 (1988) 242–247.
[40] S. Sakthivel, T. Alagesan, S. Muthu, C.S. Abraham, E. Geetha, J. Mol. Struct. 1156 (2018) 645–656.
[41] P.J. Larkin, M.P. Makowski, N.B. Colthup, Spectrochim.Acta A 55 (1999) 1011–1020.
[42] L. Bao, P. Sheng, J. Li, S. Wu, Q. Cai, S. Yao, Analyst 137 (2012) 4010–4015.
[43] H.S. Lam, A. Proctor, L. Howard, M.J. Cho, J. Food Sci. 70 (2005) C545–C549.
[44] H.A. Khamees, M. Jyothi, S.A. Khanum, M. Madegowda, J. Mol. Struct. 1161 (2018) 199–217.
[45] S. Fatma, A. Bishnoi, V. Singh, F.A. Al-Omary, A.A. El-Emam, S. Pathak, R. Srivastava, O. Prasad, L. Sinha, J.Mol.Struct 1110 (2016) 128–137.
[46] B.F. Rizwana, J.C. Prasana, C.S. Abraham, S. Muthu, J.Mol.Struct 1164 (2018) 447–458.
[47] R.M. Silverstein, G.C. Bassler, T.C. Morrill, Spectrometric Identification of Organic Compounds, John Wiley, Chichester, 1991.

[48] F.A. Cotton, C.W. Wilkinson, Advanced Inorganic Chemistry, third ed., Interscience Publisher, New York, 1972.
[49] R. Padma, M. Sathiya, S. Guhanathan, SOJ Materials Science & Engineering 15 (2017) 1–6.
[50] X.-H. Liu, Z.-X. Zhao, J. Wang, W. Zhang, H.-X. Zhang, J. Photochem. Photobiol. A: Chem. 335 (2017) 155–164.
[51] A. Uppal, Y. Khajuria, J.Mol.Struct 1179 (2019) 76–85.
[52] R.R.Muhamed M.Raja, S. Muthu, M. Suresh, J. Mol.Struct. 1128 (2017) 481–492.
[53] S.S. Khemalapure, V.S. Katti, C.S. Hiremath, M. Basanagouda, S.M. Hiremath, S.J. Armaković, S. Armaković, J. Mol.Struct. 1195 (2019) 815–826.
[54] S.I. Gorelsky, SWizard program, http://www.sg-chem.net/.
[55] K. Chaitanya, Spectrochim. Acta A. 86 (2012) 159–173.
[56] T.K. Kuruvilla, S. Muthu, J.C. Prasana, J. George, S. Sevvanthi, J. Mol. Struct. 1175 (2019) 163–174.
[57] C.Y. Panicker, K.R. Ambujakshan, H.T. Varghese, S. Mathew, S. Ganguli, A.K. Nanda, C.V. Alsenoy, J Raman Spectrosc 40 (2009) 527–536.
[58] S. Muthu, E.E. Porchelvi, Spectrochim. Acta A. 115 (2013) 275–286.
[59] G. Vengatesh, M. Sundaravadivelu, Res. Chem. Intermed. 45 (2019) 4395–4415.
[60] P. Thul, V.P. Gupta, V.J. Ram, P. Tandon, Spectrochim. Acta A. 75 (2010) 251–260.
[61] T.K. Kuruvilla, J.C. Prasana, S. Muthu, J. George, S.A. Mathew, Spectrochim. Acta A. 188 (2018) 382–393.
[62] S. Kaya, H. Gökce, T. Arslan, G. Alpaslan, J. Mol. Struct. 1202 (2020) 127270.
[63] M. Rajeshirke, N. Sekar, Optical Materials 76 (2018) 191–209.
[64] A.E. Reed, L.A. Curtiss, Chem.Soc 102 (1988) 899–926.
[65] M. Pandey, S. Muthu, N.N. Gowda, J. Mol. Struct. 1130 (2017) 511–521.
[66] C.S. Abraham, J.C. Prasana, S. Muthu, M. Raja, J. Mol. Struct. 1160 (2018) 393–405.
[67] S. Sieber, P.v.R. Schleyer, J. Gauss, J. Am. Chem. Soc. 115 (1993) 6987–6988.
[68] M. Gümüş, Y. Sert, A. Yalkın, H. Gökce, I. Koca, Chemistry Select 4 (2019) 4695–4708.
[69] H. Gokce, S. Bahceli, O. Akyildirim, H. Yuksek, O.G. Kol, Lett. Org. Chem. 10 (2013) 395–441.
[70] S. Janani, H. Rajagopal, S. Muthu, S. Aayisha, M. Raja, J. Mol. Struct. 1230 (2021) 129657.
[71] X. Liu, Y. Liu, X. Wang, T. Wang, S. Sun, W. Wang, J. Mol. Struct. 1237 (2021) 130350.
[72] H. Ishikawa, T. Sugiyama, K. Kurita, A. Yokoyama, Bioorg. Chem. 41 (2021) 1–5.
[73] S.M. Aljubiri, S.A. Mahgoub, A.I. Almansour, M. Shaaban, K.H. Shaker, Saudi J. Biol. Sci. 28 (2021) 417–426.
[74] C.I. Yeo, E.R. Tiekink, J. Chew, Inorganics. 9 (2021) 48.
[75] D.P. Singh, S.K. Deivedi, S.R. Hashim, R.G. Singhal, Pharmaceuticals 3 (2010) 2416–2425.
[76] H. Li, L. Zhang, J. Han, D. Kim, H. Kim, J. Ha, J. Wang, J. Yoon, CCS Chem. (2021) 1–30.
[77] F. Brunel, C. Lautard, C. Di Giorgio, F. Garzino, J.M. Raimundo, J.M. Bolla, M. Camplo, Bioorganic Med. Chem. Lett. 25 (2018) 926–929.
[78] F. Brunel, C. Lautard, F. Garzino, S. Giorgio, J.M. Raimundo, J.M. Bolla, M. Camplo, Bioorganic Med. Chem. Lett. 26 (2016) 3770–3773.
[79] T. Hatano, H. kagawa, T. yasuhara, T. okuda, Chem. Pharm. Bull. 36 (1988) 2090–2097.
[80] V. Suresh, N. Senthilkumar, R. Thangam, M. Rajkumar, C. Anbazhagan, R. Rengasamy, P. Gunasekaran, S. Kannan, P. Palani, Process Biochem 48 (2013) 364–373.
[81] R. Apak, M. Özyürek, K. Güçlü, E. Çapanoğlu, J. Agric. Food Chem. 64 (2016) 1028–1045.
[82] X. Li, B. Chen, H. Xie, Y. He, D. Zhong, D. Chen, Molecules 23 (2018) 1162.
[83] K.M. Amin, M.M. Ismail, E. Noaman, D.H. Soliman, Y.A. Ammar, Bioorganic Med. Chem. 14 (2006) 6917–6923.
[84] M. Ghorab, F. Ragab, H. Heiba, M. El-Gazzar, M. El-Gazzar, Acta Pharm 61 (2011) 415–425.
[85] A.Y. Elnagar, P.W. Sylvester, K.A. El Sayed, Planta. Med. 77 (2011) 1013–1019.
[86] W. Tai, T. Lu, H. Yuan, F. Wang, H. Liu, S. Lu, Y. Leng, W. Zhang, Y. Jiang, Y. Chen, J. Mol. Model. 18 (2012) 3087–3100.
[87] C.R. Maroun, T. Rowlands, Pharmacol. Ther. 142 (2014) 316–338.
[88] L. Ye, X. Ou, Y. Tian, B. Yu, Y. Luo, B. Feng, H. Lin, J. Zhang, S. Wu, Eur. J. Med. Chem. 65 (2013) 112–118.
[89] C. Li, J.J. Wu, M. Hynes, J. Dosch, B. Sarkar, T.H. Welling, M.P. di Magliano, D.M. Simeone, Gastroenterology 141 (2011) 2218–2227.
[90] O. Trott, A.J. Olson, J. Comput. Chem. 31 (2010) 455–461.
[91] B. Kramer, M. Rarey, T. Lengauer, Proteins: Struct., Funct., Bioinf 37 (1999) 228–241.
[92] S.M. Huang, R. Temple, D.C. Throckmorton, L.J. Lesko, Clin. Pharmacol. Ther. 81 (2007) 298–304.
[93] M. Gümüş, Y. Sert, A. Yalkın, H. Gökce, I. Koca, Chemistry Select 4 (2019) 4695–4708.
[94] X.Q. Li, T.B. Andersson, M. Ahlström, L. Weidolf, Drug Metab. Dispos. 32 (2004) 821–827.
[95] https://pubchem.ncbi.nlm.nih.gov/compound/11494412#section=Top.